Modeling and Transient Simulation of a Fully Integrated Multi-Pressure Heat Recovery Steam Generator Using Siemens T3000

2019

Jonathan McConnell
University of Central Florida

MODELING AND TRANSIENT SIMULATION OF A FULLY INTEGRATED
MULTI-PRESSURE HEAT RECOVERY STEAM GENERATOR USING SIEMENS T3000

by

JONATHAN MCCONNELL
B.S. University of Central Florida, 2018

A thesis submitted in partial fulfilment of the requirements
for the degree of Master of Science
in the Department of Mechanical and Aerospace Engineering
in the College of Engineering and Computer Science
at the University of Central Florida
Orlando, Florida

Summer Term
2019

ABSTRACT

The focus of this research is on the transient thermodynamic properties and dynamic behavior of a Heat Recovery Steam Generator (HRSG). An HRSG is a crossflow heat exchanger designed for the extraction of energy from the hot exhaust gas of a traditional power plant through boiling induced phase change. Superheated steam is sent through a turbine to generate additional power, raising the overall efficiency of a power plant. The addition of renewable energies and the evolution of smart grids have brought forth a necessity to gain a comprehensive understanding of transient behavior within an HRSG in order to efficiently manage the power output of traditional plants. Model-based techniques that can simulate a wide range of operating conditions can be valuable and insightful. For this reason, a multi-physics model of an HRSG has been developed in Siemens T3000 plant monitoring software. The layout and conditions of a reference HRSG have been provided by Siemens Energy Inc. along with validation data for behavioral comparison. The HRSG selected is a three pressure stage HRSG. Simultaneous simulation of these three pressure systems and their interactions has been achieved. A potential for real time execution was demonstrated. An HRSG is built of three major subsystems, namely economizers, boilers, and superheaters. A lumped control volume approach has been implemented to efficiently model the energy and mass balances of medium within each subsystem. In this effort, considering the goal of real time simulation, special attention was paid to balance computational burden with numerical accuracy.

A major focus of this research has been accurately modeling the complexities of phase change within a boiler subsystem. A switching mechanism has been developed to numerically model the dynamic heating and evaporation of boiler liquid. To increase robustness of the model to numerical fluctuations and perturbations, bidirectional flow comprising of boiling and condensation was modeled with the switching mechanism. This numerically robust model shows good agreement with the validation data provided by Siemens.

ACKNOWLEDGMENTS

I would like to give special thanks to my advisor, Dr. Tuhin Das. His guidance and support have been an essential part of my development as a researcher. I am happy to have him as a mentor and as a friend. I would like to also thank my labmates, Andres Caesar and Singith Abeysirwardena. Andres guided me to a working understanding of previous work and the inner mechanisms of T3000. He has continued to guide me from his new position at Siemens. Singith was always willing to help and mentor me as I grew as a researcher.

Furthermore, I would like to thank Prithvi Veeravalli and James Hoy for their continual support and correspondence from Siemens Energy Inc. Their guidance has played a key role in the ease and success of this research project, and I treasure not only the professional relationship, but the friendship that has grown since I gained their acquaintance. Thank you for respecting me from day one.

And of course, I would like to extend my sincere gratitude to the members of my thesis committee, Dr. Louis Chow and Dr. Tian Tian. Thank you for taking interest in my research and helping me to hold the high standard that any masters student should.

TABLE OF CONTENTS

LIST OF FIGURES

LIST OF TABLES

LIST OF ABBREVIATIONS

CV   Control Volume

Eq   Equation

HP   High Pressure

HRSG   Heat Recovery Steam Generator

IP   Intermediate Pressure

LP   Low Pressure

UFEE   Unsteady Flow Energy Equation

UI   User Interface

LIST OF SYMBOLS

A	Cross-Sectional Area	m^2
a	RK Attractive Potential Constant	$bar(\frac{m^3}{kmol})^2 K^{1/2}$
A_{F2M}	Area of Flue Gas to Metal Interface	m^2
A_{L2V}	Area of Liquid to Vapor Interface	m^2
A_{M2L}	Area of Metal to Liquid Interface	m^2
A_{M2V}	Area of Metal to Vapor Interface	m^2
b	RK Volume Correction Constant	$m^3/kmol$
C_L	Specific Heat of Liquid Water	$\frac{J}{kg*K}$
C_m	Specific Heat of Metal	$\frac{J}{kg*K}$
C_V	Specific Heat of Steam	$\frac{J}{kg*K}$
$C_{v_{fg}}$	Specific Heat of Flue Gas	$\frac{J}{kg*K}$
d	Diameter	m
ε	A Small Difference	$-$
f	Pipe Flow Friction Factor	$-$
g	Acceleration Due to Gravity	m/s^2
h_{CR}	Specific Enthalpy of Cold Reheat Steam	J/kg
h_f	Head Loss of Fluid	m
$h_{f,L}$	Specific Enthalpy of Saturated Liquid at T_L	J/kg
$h_{f,V}$	Specific Enthalpy of Saturated Liquid at T_V	J/kg
$h_{fg,in}$	Specific Enthalpy of Flue Gas Flow In	J/kg
$h_{fg,out}$	Specific Enthalpy of Flue Gas Flow Out	J/kg
H_{F2M}	Flue Gas to Metal Convective Heat Transfer Coefficient	$\frac{J}{s*m^2*K}$
$h_{g,L}$	Specific Enthalpy of Saturated Vapor at T_L	J/kg

$h_{g,V}$	Specific Enthalpy of Saturated Vapor at T_V	J/kg
h_{IP}	Specific Enthalpy of IP Steam at Cold Reheat Mixing	J/kg
h_L	Specific Enthalpy of Liquid CV	J/kg
$h_{L,in}$	Specific Enthalpy of Liquid Flow In	J/kg
$h_{L,out}$	Specific Enthalpy of Liquid Flow Out	J/kg
H_{L2V}	Liquid to Vapor Convective Heat Transfer Coefficient	$\frac{J}{s*m^2*K}$
H_{M2L}	Metal to Liquid Convective Heat Transfer Coefficient	$\frac{J}{s*m^2*K}$
H_{M2V}	Metal to Vapor Convective Heat Transfer Coefficient	$\frac{J}{s*m^2*K}$
h_{out}	Specific Enthalpy of Flow Out	J/kg
$h_{V,in}$	Specific Enthalpy of Vapor Flow In	J/kg
$h_{V,out}$	Specific Enthalpy of Vapor Flow Out	J/kg
k_f	Flow Constant	$\frac{\sqrt{kg}\sqrt{m^3}}{s\sqrt{bar}}$
$k_{f,max}$	Maximum Valve Position Flow Constant	$\frac{\sqrt{kg}\sqrt{m^3}}{s\sqrt{bar}}$
k_{temp}	Relation of IP temperature to Cold Reheat	—
L	Length	m
m	Mass	kg
$\dot{m}$	Mass Flow Rate	kg/s
$\dot{m}_{CR}$	Cold Reheat Mass Flow Rate	kg/s
m_{fg}	Total Flue Gas Mass	kg
$\dot{m}_{fg,in}$	Rate of Flue Gas Mass Flow In	kg/s
$\dot{m}_{fg,out}$	Rate of Flue Gas Mass Flow Out	kg/s
$\dot{m}_{IP}$	IP Mass Flow Rate at Cold Reheat Mixing	kg/s
m_L	Total Liquid Mass	kg

$\dot{m}_{L,in}$	Rate of Liquid Mass Flow In	kg/s
$\dot{m}_{L,out}$	Rate of Liquid Mass Flow Out	kg/s
$\dot{m}_{L2V}$	Rate of Evaporation Mass Flow	kg/s
m_m	Total Metal Mass	kg
$\dot{m}_{out}$	Rate of Mass Flow Out	kg/s
m_V	Total Vapor Mass	kg
$\dot{m}_V$	Rate of Change of Vapor Mass	kg/s
$\dot{m}_{V,des}$	Desired Rate of Change of Vapor Mass	kg/s
$\dot{m}_{V,in}$	Rate of Vapor Mass Flow In	kg/s
$\dot{m}_{V,out}$	Rate of Vapor Mass Flow Out	kg/s
$\dot{m}_{V2L}$	Rate of Condensation Mass Flow	kg/s
M_w	Molar Mass of Water	$kg/kmol$
N_V	Total Moles of Vapor	$kmol$
P_V	Vapor Pressure	bar
$P_{V,des}$	Desired Steady State Vapor Pressure	bar
P_{next}	Downstream Pressure	bar
$\dot{Q}_{F2M}$	Rate of Heat Transfer from Flue Gas to Metal	J/s
$\dot{Q}_{M2L}$	Rate of Heat Transfer from Metal to Liquid	J/s
$\dot{Q}_{M2V}$	Rate of Heat Transfer from Metal to Vapor	J/s
R	Universal Gas Constant	$\frac{J}{K*kmol}$
ρ	Density	kg/m^3
ρ_{fg}	Flue Gas Density	kg/m^3
ρ_L	Liquid Density	kg/m^3

ρ_V	Vapor Density	kg/m^3
t	Time	s
T_{CR}	Temperature of Cold Reheat Flow	K
$T_{CR_{SS}}$	Steady State Temperature of Cold Reheat Flow	K
$T_{fg,avg}$	Average Flue Gas Temperature	K
$T_{fg,in}$	Flue Gas Input Temperature	K
$T_{fg,out}$	Flue Gas Output Temperature	K
$\dot{T}_{fg,out}$	Rate of Flue Gas Output Temperature Change	K/s
T_{IP}	Temperature of IP Flow at Cold Reheat Mixing	K
$T_{IP_{SS}}$	Steady State IP Flow Temperature	K
T_L	Temperature of Liquid CV	K
$\dot{T}_L$	Rate of Liquid Temperature Change	K/s
T_m	Temperature of Metal CV	K
$\dot{T}_m$	Rate of Metal Temperature Change	K/s
T_{sat}	Saturation Temperature	K
T_V	Temperature of Vapor CV	K
$\dot{T}_V$	Rate of Vapor Temperature Change	K/s
u	Specific Internal Energy	J/kg
$u_{g,V}$	Specific Internal Energy of Saturated Vapor at T_V	J/kg
u_L	Specific Internal Energy of Liquid CV	J/kg
u_V	Specific Internal Energy of Vapor CV	J/kg
v	Molar Specific Volume	$m^3/kmol$
V_{fg}	Flue Gas Volume	m^3

V_L	Liquid Volume	m^3
V_{total}	Total Volume	m^3
V_V	Vapor Volume	m^3
$\dot{X}$	Fluid Velocity	m/s
Z	Volumetric Contribution to Change in Internal Energy	J/s

CHAPTER 1: INTRODUCTION

1.1 Research Motivation

As the world takes strides toward more complex and diverse methods of producing electrical power, it is necessary to gain a detailed understanding of current technologies in order to ease the transition to greener energy. Many renewable energy sources, like wind and solar power, do not output a consistent amount of power, and will fluctuate drastically throughout a given day-night cycle. This contrasts to current traditional power plants, as most have been designed only for full power output. In regions with a high density of renewable energy sources, it falls on the shoulders of traditional power plants to even out the power supplied to the grid. As it is damaging to send too much power to the grid at any given time, traditional power plants must be dynamically powered up and down to fulfill the demand of the given area. This dynamic power regulation calls for a detailed understanding of the transient behavior observed within a traditional power plant. Thus, accurately modeling this behavior is key to understanding the nuances of a fluctuating traditional power plant. Study of such a model can help to develop efficient methods for power regulation that not only benefit traditional power plants, but reduce the environmental impact of these older technologies.

1.2 Research Objectives

This research focuses on Heat Recovery Steam Generators (HRSG). A thorough description of an HRSG will be given in Chapter 2. The goal of this research is to create a dynamic, transient simulation of an entire multi-pressure HRSG. This model will accurately capture the transient behavior and steady state thermodynamic properties of an HRSG given input conditions characteristic of

an actual HRSG system. A major challenge of this research will be the development of a robust boiler model. The two phases of water present in a boiling system require careful attention to the mass flow and heat transfer interactions between phases. By directly modeling individual physical phenomena, this research aims to create a simple yet robust transient simulation that can be easily implemented into a plant control system.

The simulation results of this HRSG model will be validated against the real trends of a reference HRSG provided by Siemens Energy Inc. The main goal of this research is to model realistic, physics-based behavior in all subsystems of an HRSG. This behavior should be insightful and predictive for a variety of HRSG configurations and input conditions. It follows that the resulting trends of the HRSG model should display similar behavior to those shown in the reference data.

1.3   Research Approach

A model will be simulated using Siemens T3000 plant monitoring software. An overview of T3000 modeling will be presented in Chapter 2. The model presented in this research will be an adaptation and improvement of the foundational model presented in [1]. This previous work will be discussed in Chapter 3. An overview of the structure and numerical calculations of the aforementioned T3000 model will be presented in detail in Chapters 5 and 6. This research will focus on developing a model of each individual subsystem using first principle calculations on lumped control volumes (CV). Discretization of calculations will allow for individual analysis of subsystems while capturing the connections and thermodynamic interplay observed in an entire HRSG in a manner consistent with the underlying physics.

CHAPTER 2: BACKGROUND INFORMATION

2.1   Heat Recovery Steam Generators

A Heat Recovery Steam Generator (HRSG), seen in Figure 2.1, [2], is a counter flow heat exchanger added in series to traditional power plants to increase efficiency. The exhaust from gas or coal burning power plants (also known as "Flue Gas") contains a significant amount of energy in the form of heat. An HRSG uses this extra heat to boil water into steam, and pass said steam through secondary turbines. This process works to create a more efficient power plant, and reduces the temperature of the exhaust gas before it is released to the atmosphere. The flue-gas-to-water heat exchange is broken down into three major sections for each pressure stage. The economizer raises liquid feed water to just below saturation. The boiler evaporates the preheated water into steam. The superheater heats the steam past saturation to add more energy and ensure no water droplets are sent through the steam turbine.

Figure 2.1: OUTSIDE VIEW OF HEAT RECOVERY STEAM GENERATOR
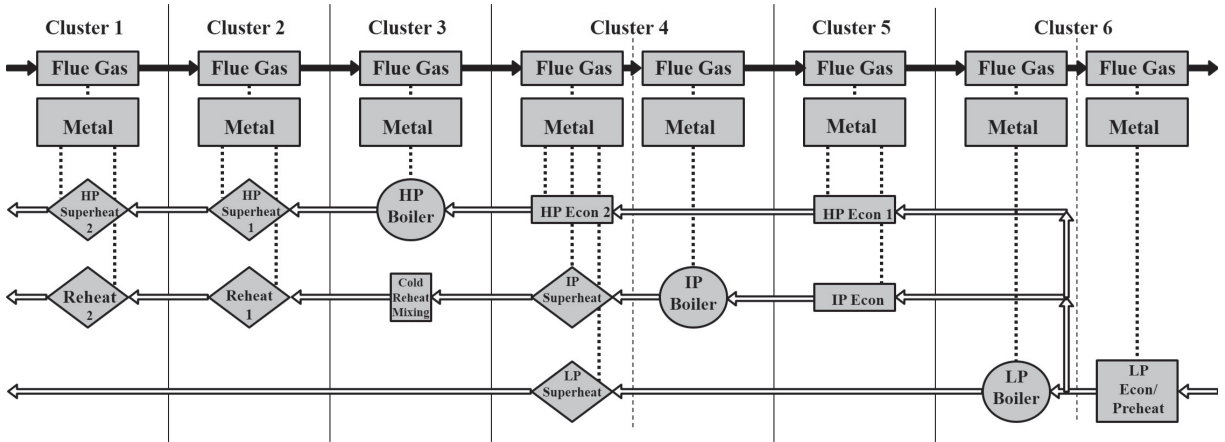
Figure 2.2: SCHEMATIC OF HRSG SYSTEM

The Siemens HRSG used for reference in this research has three separate pressure systems: Low Pressure (LP), Intermediate Pressure (IP), and High Pressure (HP). Each of these pressure systems is built of different combinations of economizers, boilers, and superheaters. The water and steam pipes of the reference HRSG are organized in clusters. The subsystems included in each cluster are known to have similar steady state temperatures. Thus, the subsystems must interact with similar flue gas temperatures. Figure 2.2 shows a flow chart representation of the reference HRSG. The clusters are displayed as columns of the flow chart and are numbered 1 through 6. In this notation, Cluster 1 interacts with the hottest flue gas. Each subsequent cluster interacts with flue gas of lower temperature as heat is exchanged with previous subsystems. This nomenclature will be used for the duration of the document.

2.2   Modeling in T3000

T3000 is a two dimensional user interface (UI) that uses flowchart diagrams to perform logic and calculations in real time. This program was originally developed by Siemens Energy Inc. to serve as a plant monitoring software.

4
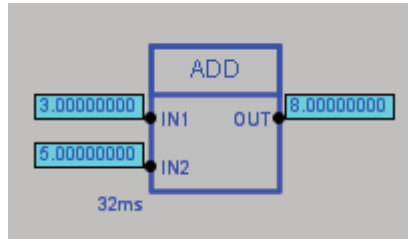
Figure 2.3: EXAMPLE CALCULATION BLOCK

Previous research has been conducted to validate T3000's ability to handle large scale transient simulation [1]. This chapter will provide a brief overview of designing a calculation in T3000. This will provide insight into the simulation process used to solve the equations in later chapters.

2.2.1   Basic Calculations

Base level calculations in T3000 are performed by individual blocks, taking in inputs and sending out outputs as shown in Figure 2.3. These calculations can be numerical or logic based for use in conditional statements. Along with conditional operators, there are also many more complex features such as integral blocks and look up tables. Simple calculations can be assembled in series and parallel chains to model governing equations including algebraic as well as differential equations. T3000 performs all calculations in a created chain every cycle of simulation.

2.2.2   Example Module

The previously mentioned complex chains of calculations can be condensed into higher level modules. An example module is shown in Figure 2.4. These higher level modules are used for organization and separation of the calculations associated with each CV.
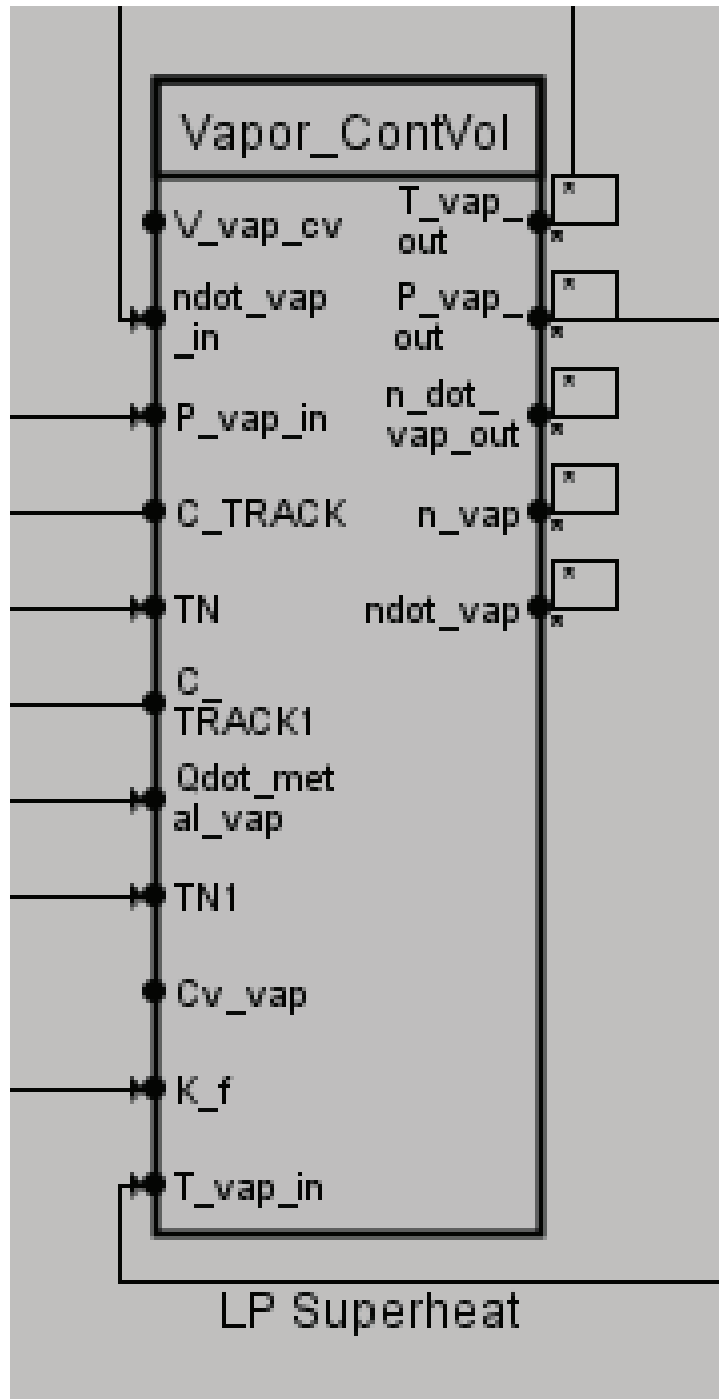
Figure 2.4: EXAMPLE MODULE BLOCK

CHAPTER 3: PREVIOUS WORKS

A significant amount of previous research has been devoted to exploring boiler dynamics. High fidelity finite element simulations can produce finely detailed descriptions of boiler behavior, [3]. However, such a complex model is too computationally demanding for the purposes of plant control. For this reason, many researchers have explored the concept of a simplified boiler model for use in control of boiler system parameters in real time. Notable work in this field has demonstrated the practicality of a first principle, non-linear boiler model for use in drum-boiler control, [4], [5], [6]. It has been shown that a lumped parameter model can produce reasonable results while maintaining low complexity and minimizing computational burden, but early models of such classification have worked around the issue of directly modeling phase change, [7]. In [8], saturation conditions are assumed, and saturated steam and water parameters are assumed to be a function of boiler pressure. These boiler models, while successful in their own regard, leave further room for simplification. With the goal of modeling an entire HRSG system, the complexity of a given model is compounded with the multiplicity of subsystems. Therefore, it is imperative that a boiler model be optimized to reduce the collective computational burden of an HRSG model.

Other research has been conducted on modeling an entire HRSG, [9], [10], [11]. The early model presented in [9] relies directly on the incorporation of parameter profiles for many significant subsystems. Though accurate for modeling a specific system in a specified regime, this model lacks versatility when considering new input profiles or perturbation.

In direct relation to this research, a preliminary foundation has been developed. An initial model of each pressure system has been separately developed for incorporation in a fully integrated model. These initial models will be discussed below.

3.1 Low Pressure System

The LP system consists of an economizer, a boiler, and a superheater. The lack of duplication in subsystems made the LP system an obvious starting point for building the HRSG model. A complete T3000 model of the LP system was developed by Caesar in 2018, [1]. This model is displayed in Figure 3.1. The model was constructed using lumped CVs for flue gas, metal, liquid (water), and vapor (steam). Heat transfer calculations are performed to balance the energy transferred across interfaces. The LP system is the least volatile of the three pressure systems, and as the name suggests, the pressures and energies associated with the LP system are quite low compared to the other pressure systems.
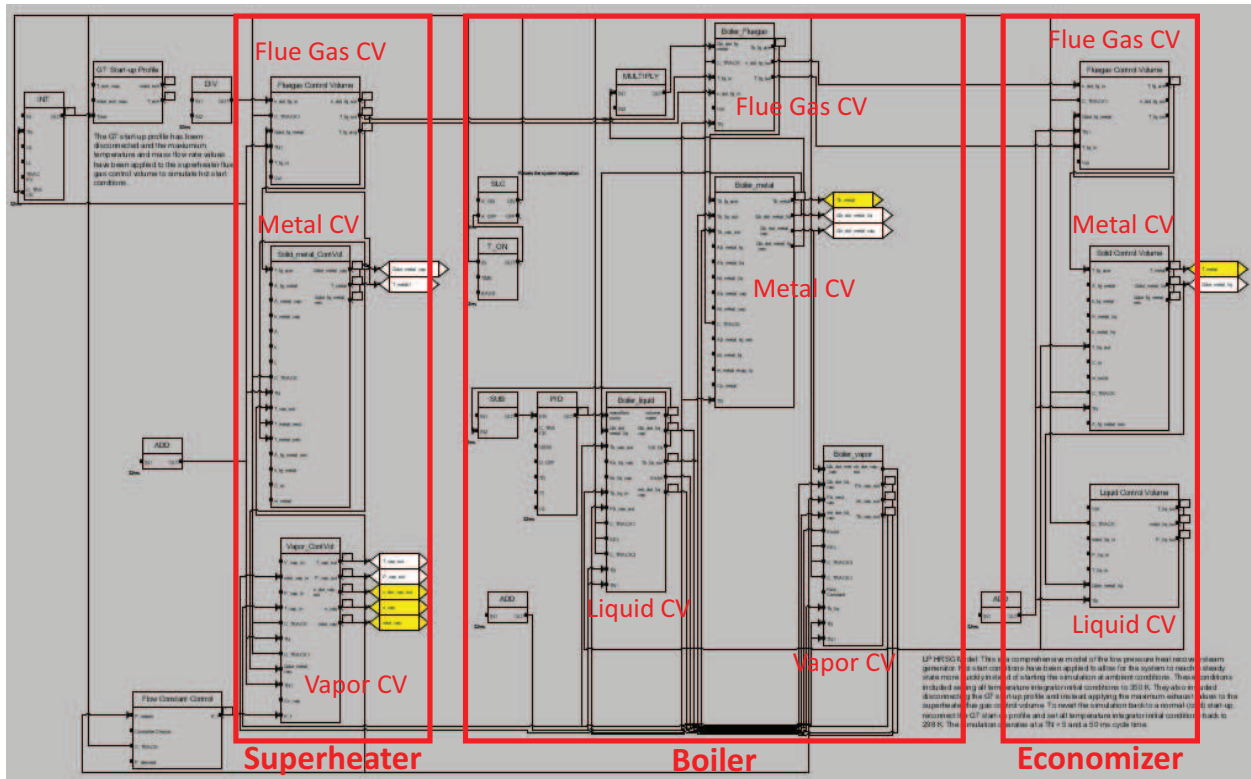
Figure 3.1: LOW PRESSURE T3000 MODEL

It was reasonable to approximate the boiler pressure as saturation pressure at the given vapor temperature. After tuning heat transfer parameters, it was found that this lumped CV model shows good agreement with start-up transient trends as well as steady state values from actual plant data.

3.2   High Pressure System

The HP System is a larger system containing two economizers, a larger boiler, and two super-heaters. Also, as the name implies, the steady state pressure of the HP system is significantly greater than that of the LP. The method implemented for the LP system was scaled to include the extra subsystems included within the HP system. A complete T3000 model of the HP system is displayed in Figure 3.2. This initial model was partially successful, but was prone to significant numerical oscillations and non-realistic behavior. For this reason it was necessary to refine the boiler model (which will be presented in detail in Chapter 6) to create a more robust and more accurate HRSG model.
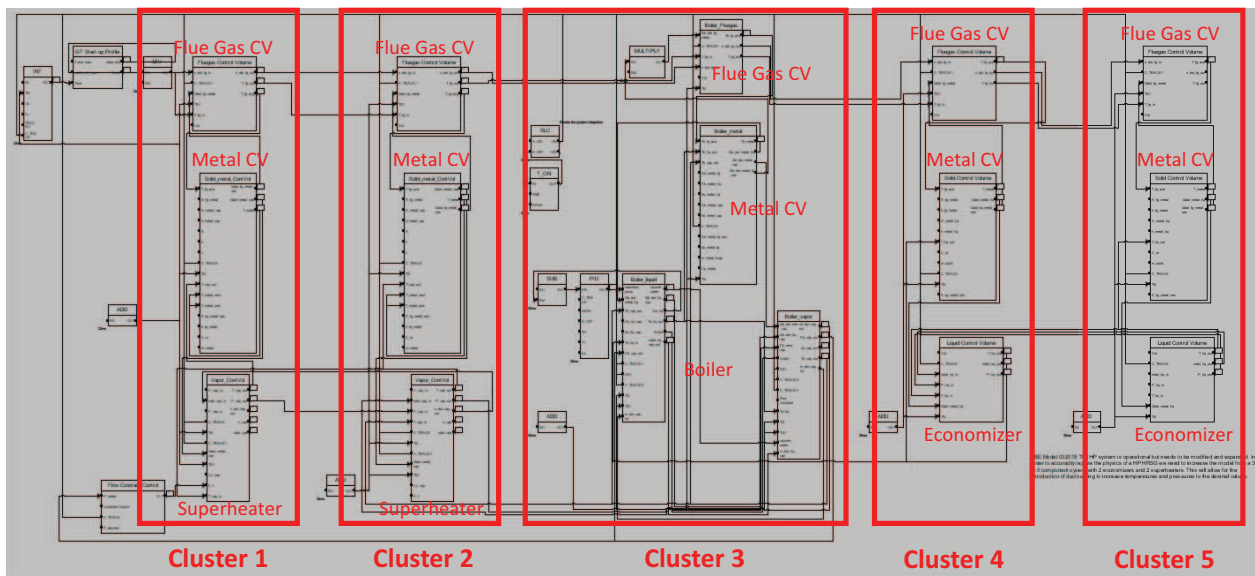
Figure 3.2: HIGH PRESSURE T3000 MODEL

CHAPTER 4: FULLY INTEGRATED MODEL

4.1 Combined High and Intermediate Pressure Model

The Intermediate Pressure (IP) System consists of an economizer, a boiler, and three superheaters. The implementation of the T3000 model to the IP System is not as straight forward as that of the LP and the HP systems. This is largely due to the significant coupling of the HP Exhaust and the IP steam flow, seen in Figure 4.1 as "Cold Reheat Mixing". For accurate simulation of the coupling effect, it is necessary to simultaneously simulate the HP and IP systems in the same model. As opposed to a direct doubling of simulation complexity, the flue gas and metal CVs can be further lumped.
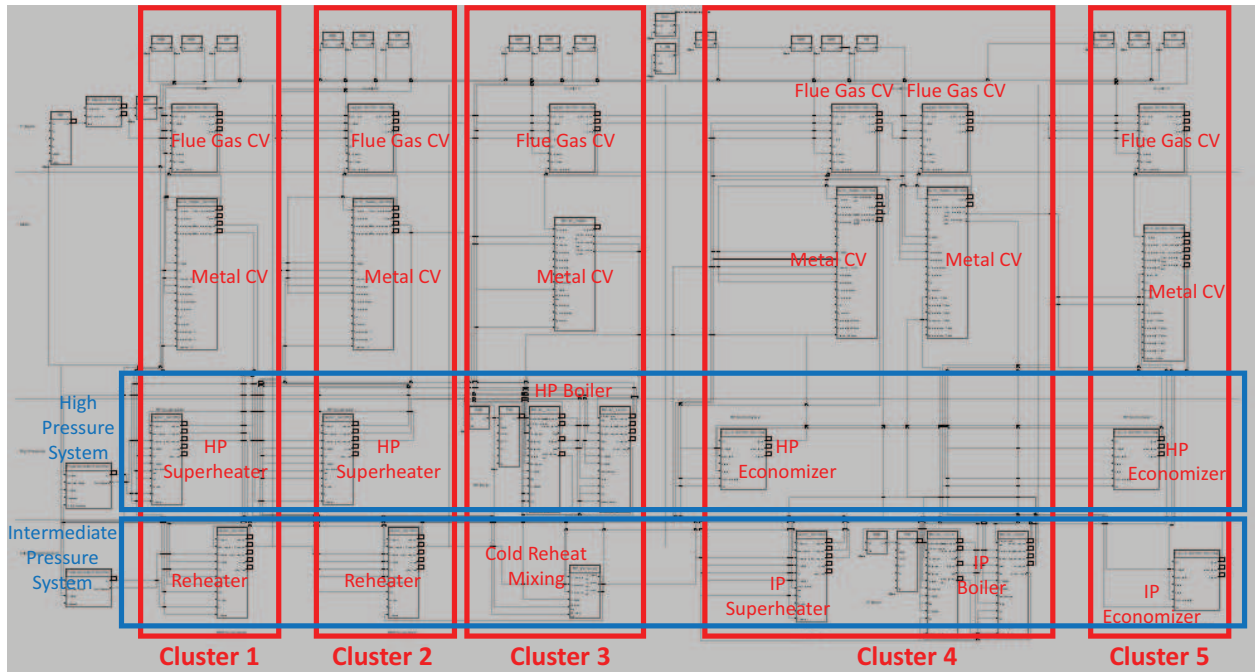
Figure 4.1: COMBINED HIGH AND INTERMEDIATE PRESSURE T3000 MODEL

The HRSG used for reference in constructing this T3000 model has pipes bundled into clusters. Each cluster has been designed so that the contents of the contained pipes are at similar steady state temperature. This phenomenon is emphasized by the overlapping of cycles seen in the T-S Diagram of a similar HRSG shown in Figure 4.2, [12]. It is therefore reasonable to use one lumped flue gas and one lumped metal CV for each cluster. With the lumped metal CV model, it is assumed that the entire mass of metal making up the pipes in each cluster is at one uniform temperature. This assumption is sufficient in the majority of clusters, but causes significant inaccuracies for clusters containing two or more subsystems from the same pressure system, i.e. Cluster 4, seen in Figure 4.1. For this special case, it is necessary to split the flue gas and metal CVs further to achieve higher fidelity of temperature distribution.
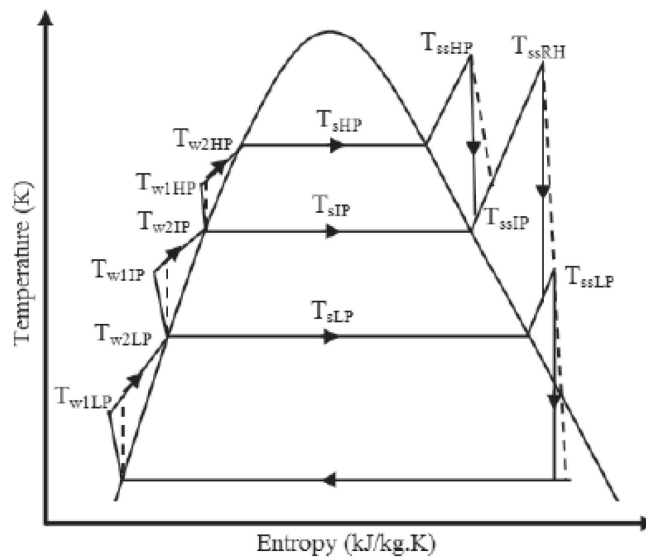
Figure 4.2: TS DIAGRAM OF MULTI-STAGE HRSG

4.2 Combined High, Intermediate, and Low Pressure Model

The logical next step to the HP and IP combined model is to add the LP system, creating a Fully Integrated Model. Similarly to the IP system, the LP system has two subsystems within one cluster, and thus Cluster 6 must be split in two, as was done for Cluster 4. It should be noted that, in the reference HRSG, the LP economizer is used to preheat the liquid medium of the entire HRSG before it is distributed proportionally to each pressure system. This coupling is incorporated into the Fully Integrated Model and can be observed in the T3000 model presented in Figure 4.3.
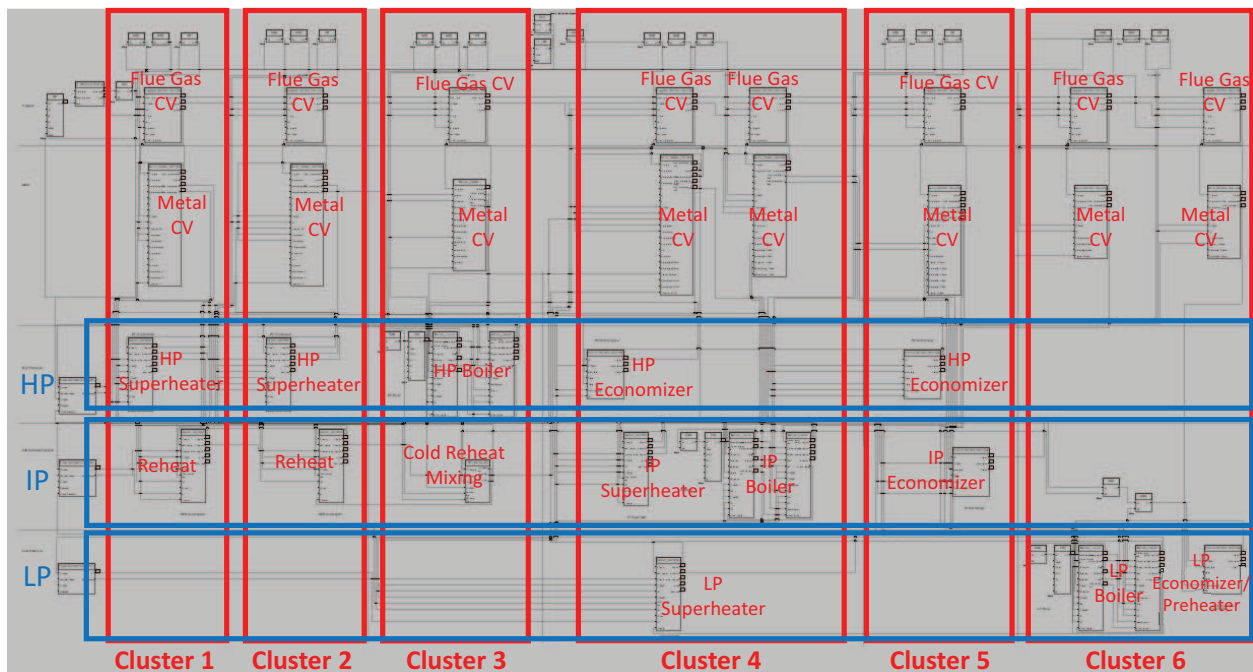
Figure 4.3: FULLY INTEGRATED T3000 MODEL

CHAPTER 5: HRSG MODEL

5.1 Flue Gas Control Volume

The flue gas within an HRSG is near to atmospheric pressure and experiences negligible pressure drops throughout the HRSG. For this reason, the mass within each flue gas CV is taken to be constant, leading to the mass balance equation seen in Eq. (5.1).

$$\dot{m}_{fg,in} = \dot{m}_{fg,out} \tag{5.1}$$

This assumption allows for the total flue gas mass to be calculated directly from geometric conditions, shown in Eq. (5.2).

$$m_{fg} = V_{fg}\rho_{fg} \tag{5.2}$$

The purpose of the presented HRSG model is to track transient conditions. This goal cannot simply be achieved through the use of static energy balance equations. It is instead necessary to consider the Unsteady Flow Energy Equation (UFEE) when evaluating the parameters of a CV within the model. The UFEE is presented qualitatively in Eq. (5.3).

$$\frac{d(mu)}{dt} = (enthalpy\ of\ mass\ in) - (enthalpy\ of\ mass\ out) + (heat\ in) \tag{5.3}$$

5.1.1 Temperature Averaging

For the flue gas CV, Eq. (5.3) can be arranged as shown in Eq. (5.4).

$$m_{fg}C_{v_{fg}}\dot{T}_{fg,out} = \dot{m}_{fg,in}(h_{fg,in} - h_{fg,out}) - \dot{Q}_{F2M} - \dot{Q}_{amb} \tag{5.4}$$

The rate of change of the flue gas temperature can be calculated by rearranging Eq. (5.4) to solve for the appropriate term, as seen in Eq. (5.5),

$$\dot{T}_{fg,out} = \frac{\dot{m}_{fg,in}(h_{fg,in} - h_{fg,out}) - \dot{Q}_{F2M} - \dot{Q}_{amb}}{m_{fg}C_{v_{fg}}}, \qquad (5.5)$$

where $\dot{Q}_{F2M}$ is the heat transferred from the flue gas to the metal pipes at a given section of the HRSG. This heat transfer is convective and thus, can be represented by Eq. (5.6).

$$\dot{Q}_{F2M} = H_{F2M}A_{F2M}(T_{fg,avg} - T_m) \qquad (5.6)$$

In Eq. (5.6), H_{F2M} and A_{F2M} are the convective heat transfer coefficient and the surface area, respectively, of the flue gas to metal interface.

A significant temperature drop is observed across each flue gas CV. For this reason, it is necessary to consider an average temperature, $T_{fg,avg}$, for more accurate simulation of the heat exchange at the interface of the flue gas and the metal pipes. For ease of modeling, a simple average has been performed, as shown in Eq. (5.7).

$$T_{fg,avg} = \frac{T_{fg,in} + T_{fg,out}}{2} \qquad (5.7)$$

The value of $T_{fg,out}$ can be found by integrating Eq. (5.5).

It is important to note that this temperature averaging is an approximation of the true flue gas/metal interaction. One significant side effect of this approximation is an over estimation of flue gas temperature in response to a step down in input temperature. Looking at the presented flue gas equations from a strictly mathematical perspective, an the input temperature lower than the temperature of the metal CV pushes the output temperature, $T_{fg,out}$, to a temperature higher than the metal temperature. The model will attempt to reach an equilibrium between $T_{fg,avg}$ and T_m, as these

14

temperatures are present in the heat transfer equation. In reality, it is impossible for the output temperature of the flue gas CV to be greater than the metal temperature. Thus, it is important to put a hard ceiling on the output temperature at the value of the metal temperature, i.e. $T_{fg,out} \leq T_m$.

5.1.2 Ambient Heat Loss

It was observed in initial simulations that steady state values comparable to those provided in the reference data were achieved while removing less heat from the flue gas than was suggested by the data. For this reason, it is necessary to consider a heat loss to the environment surrounding the HRSG. This heat loss is represented by Eq. (5.8).

$$\dot{Q}_{amb} = H_{amb}A_{amb}(T_{fg,avg} - T_{amb}) \tag{5.8}$$

In this equation, ambient heat loss is combined to a single convective heat loss through the surface area of the inside of the HRSG associated with each flue gas CV. H_{amb} is assumed to be consistent throughout the HRSG. The ambient temperature, T_{amb} is assumed to be at room temperature, 298 K. It was found that the addition of this term allowed for more comparable temperature to be achieved within the flue gas CVs while maintaining accurate steady state approximations within the water and steam CVs of each subsystem.

5.2   Metal Control Volume

The metal pipes are assumed to be uniform temperature throughout the mass. With this assumption, the rate of change in temperature for the metal is a function of the conduction at the two interfaces: flue gas to metal and metal to medium. For the metal CV, no flow is present. Thus, an energy

conservation calculation can be performed, as presented in Eq. (5.9).

$$m_m C_m \dot{T}_m = \dot{Q}_{F2M} - \dot{Q}_{M2L} \qquad (5.9)$$

Eq. (5.9) can be rearranged to find the rate of change of the metal temperature, as displayed in Eq. (5.10).

$$\dot{T}_m = \frac{\dot{Q}_{F2M} - \dot{Q}_{M2L}}{m_m C_m} \qquad (5.10)$$

The uniform temperature of the metal can be found by integrating Eq. (5.10).

It should be noted that Eq. (5.10) refers to an interaction between metal and liquid. In the case of a vapor medium, $\dot{Q}_{M2L}$ should be replaced by a corresponding $\dot{Q}_{M2V}$. This rate of heat transfer from metal to liquid can be solved for using the convective heat transfer equation shown in Eq. (5.11),

$$\dot{Q}_{M2L} = H_{M2L} A_{M2L} (T_m - T_L), \qquad (5.11)$$

where H_{M2L} and A_{M2L} represent the convective heat transfer coefficient and the surface area, respectively, of the metal to liquid interface.

Once again, Eq. (5.11) represents a metal to liquid interaction. In the case of a metal to vapor interaction, $\dot{Q}_{M2V}$, the terms H_{M2L}, A_{M2L}, and T_L should be replaced by H_{M2V}, A_{M2V}, and T_V, respectively.

5.3   Economizer Model

The Economizer is designed to heat feed water to near saturation conditions before entering the boiler, and thus, it is comprised of a single liquid CV. The liquid CV is considered to be incompressible, enforcing that the mass flow in to the CV be equal to the mass flow out, as presented in

Eq. (5.12).

$$\dot{m}_{L,in} = \dot{m}_{L,out} \tag{5.12}$$

In turn, the total mass of the liquid CV can be calculated from the volume of the economizer subsystem using Eq. (5.13).

$$m_L = V_L \rho_L \tag{5.13}$$

With the assumption of incompressibility, the UFEE can be arranged as shown in Eq. (5.14)

$$m_L C_L \dot{T}_L = \dot{m}_{L,in}(h_{L,in} - h_{L,out}) + \dot{Q}_{M2L} \tag{5.14}$$

Eq. (5.14) can be rearranged to calculate the rate of change in temperature, as seen in Eq. (5.15).

$$\dot{T}_L = \frac{\dot{m}_{L,in}(h_{L,in} - h_{L,out}) + \dot{Q}_{M2L}}{m_L C_L} \tag{5.15}$$

The temperature of the liquid CV can be found by integrating Eq. (5.15). For liquid water, the pressure contribution to the enthalpy is considered negligible, thus the pressure need not be calculated for the economizer. This assumptions also in turn assumes the enthalpy to be equal to the internal energy of the liquid, i.e. $h_L = u_L$.

It should be noted that the pressures within an HRSG are much greater than the pressure change due to hydrostatic pressure within the pipes. For this reason, the model assumes the effect of hydrostatic pressure to be negligible.

5.4   Boiler Model

As the Boiler model is quite complex and has been a major focus of the author's novel development upon previous HRSG models, the Boiler model will be discussed in length in Chapter 6.

5.5 Superheater Model

The Superheater serves to heat saturated steam to superheated steam before it is discharged to the steam turbine. A single vapor CV is considered in the model of the superheater. Given the compressible nature of a vapor CV, it is necessary to perform both energy and mass balance, as well as a pressure calculation. The mass balance can be solved to find the change in mass of the vapor CV, as shown in Eq. (5.16).

$$\dot{m}_V = \dot{m}_{V,in} - \dot{m}_{V,out} \tag{5.16}$$

$$\dot{m}_{V,out} = k_f \sqrt{\rho_V} \sqrt{P_V - P_{next}} \tag{5.17}$$

Eq. (5.16) can be integrated to find the total mass of the vapor CV.

For a superheater subsystem, the UFEE can be arranged, as presented in Eq. (5.18).

$$m_V C_v \dot{T}_V = \dot{m}_{V,in}(h_{V,in} - u_V) - \dot{m}_{V,out}(h_{V,out} - u_V) + \dot{Q}_{M2V} \tag{5.18}$$

The rate of change of the vapor temperature in the superheater can be calculated by rearranging Eq. (5.18) as shown in Eq. (5.19).

$$\dot{T}_V = \frac{\dot{m}_{V,in}(h_{V,in} - u_V) - \dot{m}_{V,out}(h_{V,out} - u_V) + \dot{Q}_{M2V}}{m_V C_v} \tag{5.19}$$

Eq. (5.19) can be integrated to find the temperature of the vapor CV. As previously mentioned, it is necessary to also calculate the pressure of the vapor CV. The high temperature and high pressure regime of the steam observed in the HRSG is accurately modeled by the Redlich-Kwong equation of state (RK), [13]. The pressure can be calculated directly using Eq. (5.20).

$$P_V = \frac{RT_V}{v - b} - \frac{a}{\sqrt{T_V} v(v + b)} \tag{5.20}$$

It should be noted that v is the molar specific volume of the vapor, and a and b are constants of the RK equation.

5.5.1 Throttle Valve

Eq. (5.17) represents the vapor flow allowed through a given set of pipes from one subsection to the next. k_f is a flow constant representing the ease/restriction of mass flow. Special attention must be paid to this value, as it is important to accommodate the geometric and system properties of each transitional section. For instance, in pipes with a larger amount of flow, it is necessary to have a large k_f value to avoid an unrealistically high resistance to flow. On the contrary, a region of lesser flow requires a lower k_f value in order to effectively build up pressure. A step-by-step derivation of k_f can be seen in Appendix A.

One special case is seen at the outlet of the final superheater in each pressure system. Upon start-up, limited vapor supply and low energy medium conditions require that no material be initially sent to the steam turbine. A valve is kept closed for the purposes of building pressure. When pressure reaches a selected threshold, the valve is opened slowly to regulate flow until the system reaches full capacity. This phenomenon is captured in the model through a dynamic adjustment of the k_f value associated with the flow out of the final superheater. k_f is held at a small value (it was found that setting the flow constant to zero would cause numerical issues) until the system reaches the pressure specified by Siemens valve control data. When the pressure is sufficient, a first order filter is used to slowly raise the k_f value to a maximum value as the system approaches full capacity. This maximum value can be found through a reverse calculation of Eq. (5.17) using the desired steady state values of the pressure system, as presented in Eq. (5.21).

$$k_{f,max} = \frac{\dot{m}_{V,des}}{\sqrt{\rho_V}\sqrt{P_{V,des} - P_{next}}} \qquad (5.21)$$

19

In Eq. (5.21), ρ_V is the density of the vapor taken at the desired steady state conditions.

The time selected to reach steady state must be properly tuned to fit the rate at which each pressure system reaches full capacity. A slow valve opening will falsely elongate the behavior of the pressure system, where as a fast valve opening time has been observed to cause oscillations in the pressure.

5.6   Miscellaneous HRSG Features

5.6.1   Preheater

The LP economizer of the reference HRSG is used to not only preheat the the LP liquid flow, but the entire feed water flow of the HRSG system. This preheated water is later split to be sent to the LP boiler, the HP economizer, and the IP economizer. This produces a strong thermodynamic coupling for all initial liquid CVs. This coupling is appropriately modeled in the T3000 diagram. The mass flow seen by the LP economizer is that of the entire HRSG, and the input temperature of the initial IP and HP economizers is the output temperature of the LP economizer.

5.6.2   Cold Reheat Mixing

After the superheated HP steam has passed through the HP steam turbine, the flow is diverted to join with the IP steam flow between the IP superheater and the first reheater (shown in the flowchart diagram in Figure 2.2). This has several significant implications. First, the HP system is not discharged to atmospheric pressure, but is instead discharged to the current pressure of the IP system. At the same time, the flow entering the reheater is significantly greater than that leaving the IP superheater. This mixing must be dynamically modeled to properly display the behavioral

coupling of the HP and IP system.

The current research has not included a steam turbine model, and thus the properties of the HP exhaust must be approximated. The pressure is assumed to be the pressure of the IP system at the point of mixing. Through out the entirety of the model simulation, the mass flow output of the mixing juncture can be calculated with a simple mass balance, as presented in Eq. (5.22).

$$\dot{m}_{out} = \dot{m}_{IP} + \dot{m}_{CR} \tag{5.22}$$

Here, "CR" stands for "Cold Reheat" which represents the HP exhaust after passing through the HP steam turbine. The gaseous interaction in question is that of real gases, given their high temperature and high pressure at steady state. For this reason, temperature cannot be calculated from a simple mass weighted average. Instead, an enthalpy balance must be performed, as shown in Eq. (5.23).

$$\dot{m}_{out}h_{out} = \dot{m}_{IP}h_{IP} + \dot{m}_{CR}h_{CR} \tag{5.23}$$

Eq. (5.23) can be solved to find the enthalpy of the out-flowing steam, as shown in Eq. (5.24).

$$h_{out} = \frac{\dot{m}_{IP}h_{IP} + \dot{m}_{CR}h_{CR}}{\dot{m}_{out}} \tag{5.24}$$

The input enthalpies are the respective enthalpies associated with each input flow temperature. Due to a lack of transient data, the mixing of the IP flow and the HP exhaust must be modeled in three piecewise stages. At start-up of the HRSG there is initially no mass flow from the system, as the contents of the boilers have not yet reached saturation condition. In this region of the simulation, Eq. (5.24) cannot be relied on as the denominator of the equation will be zero. For this reason, the temperature calculation is bypassed, and the output temperature is assumed to be that of the IP system. This assumption is reasonable as there is currently no contribution from the HP exhaust.

When the HP boiler begins to send steam through the HP pressure system (which for the most part happens before the IP boiler reaches saturation), the denominator of Eq. (5.24) is no longer zero. The temperature of the output steam is the temperature associated with the pressure and the enthalpy calculated in Eq. (5.24). The remaining unknown is the input temperature of the HP exhaust. Two separate methods can be used to approximate this temperature. The data provided by Siemens denotes the steady state temperature of the incoming exhaust. With this information, the temperature of the exhaust can be assumed to have a direct relationship to the temperature of the IP system proportionally equal to the relation of the two temperatures at steady state, as presented in Eqs. (5.25) and (5.26).

$$T_{CR} = k_{temp} T_{IP} \tag{5.25}$$

$$k_{temp} = \frac{T_{CR_{SS}}}{T_{IP_{SS}}} \tag{5.26}$$

This approximation is accurate at steady state, but produces a temperature that is too high at start-up. For this reason, the temperature of the exhaust at start-up can be assumed to be the current temperature of the final HP superheater. A logical block can be used to select the smaller of these two values to produce a reasonable temperature curve during simulation.

Figure 5.1 shows the profile produced by the logical procedure presented in this section. There is an initial spike in temperature due to small, erroneous fluctuations in system values upon start-up. The effect of this error is negligible as no mass flow is present. After initial fluctuations have settled, the mixing model follows the temperature of the IP input until approximately 12 minutes of simulated time. At this time, HP mass flow begins and the enthalpy calculation takes over. The HP exhaust temperature is assumed to be consistent with the steam temperature at the exit of the final HP superheater until approximately 30 minutes of simulated time. From this point onward, the HP exhaust temperature is approximated by Eq. (5.25).
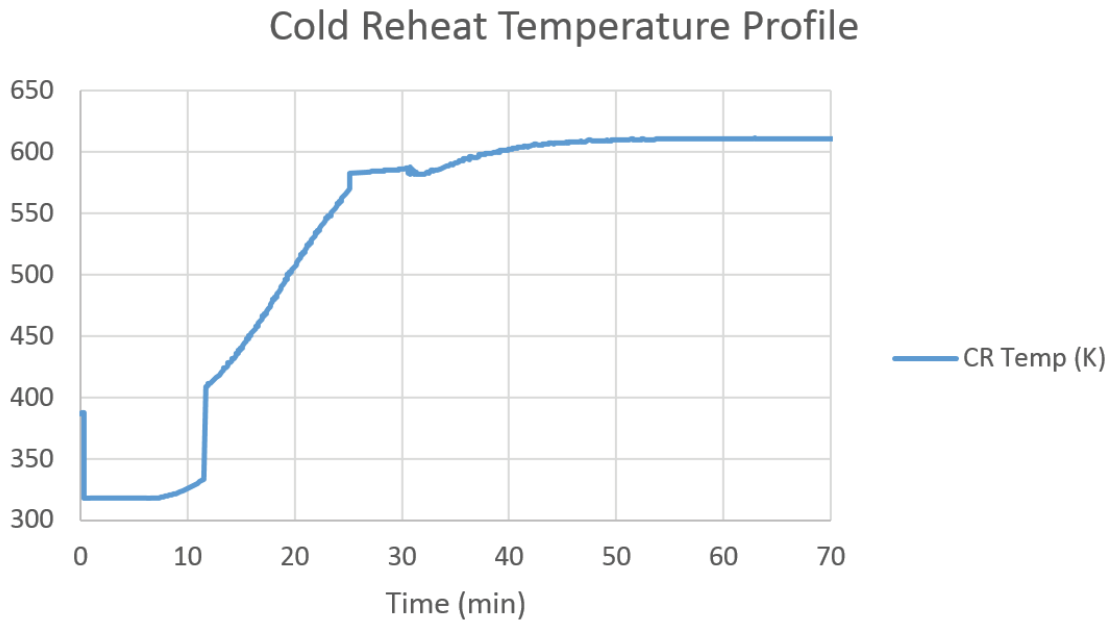
Figure 5.1: COLD REHEAT TEMPERATURE PROFILE PARTIAL CAPACITY

It should be noted that this mixing model could be improved with the addition of a CV to represent the junction point. In the case of this research, there is a lack of geometric information pertaining to the Cold Reheat junction, and thus it is necessary to make an enthalpy balance approximation. It should also be noted that the introduction of an additional CV would require the inclusion of several new integral calculations. This added complexity is an unnecessary computational load for the additional accuracy it would provide.

5.6.3 Thermodynamic Interplay

Modeling the entire HRSG system sheds light on the thermodynamic coupling of all three pressure systems. This is easily seen through the tuning of heat transfer coefficients. The medium within the pipes and the flue gas outside the pipes ultimately flow in opposite directions. This means that

23

a change in one location of the HRSG will effect the behavior of the entire HRSG model. For example, if one were to adjust the heat transfer coefficient of a superheater, one may assume that this will not effect the behavior of the boiler as it is downstream. This is false, as the superheater adjustment will change the amount of energy left in the flue gas before it reaches the boiler. In extreme cases, the down stream subsystems can draw so much energy from the flue gas that the upstream subsystems will be choked off and not perform efficiently. On the contrary, if one were to make a heat transfer coefficient adjustment upstream in the system, for instance in an economizer, this will effect the energy in the medium as it propagates further through the system. This complex phenomenon calls for careful analysis of perturbation response when tuning the system parameters to better fit the behavior of reference data.

CHAPTER 6: BOILER MODEL

6.1 General Layout

The boiler is the most complex and numerically intensive subsystem within each pressure system. In the presented model, a separate liquid and vapor CV are considered, each with their own energy and mass balance. These CVs are coupled through phase-change mass transfer and heat transfer at the shared boundary.

6.1.1 Switching Mechanism

The key physical phenomenon which sets the boiler subsystem apart from other majors subsystems within the HRSG model is phase change. This phenomenon adds an extra mass flow which must be calculated in order to perform proper energy and mass balancing within each CV.
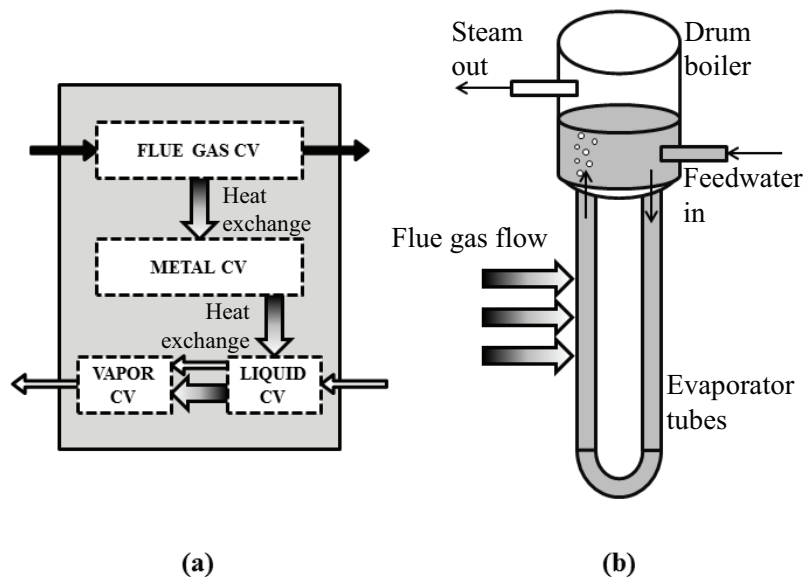

(a)   **(b)**

Figure 6.1: VISUAL REPRESENTATION OF BOILER MODEL

Fortunately for the sake of calculation, temperature of the respective CV can be assumed constant during a phase change. This assumption effectively allows the same number of equations to be solved as was utilized in the calculations for simpler systems like the Superheater. The difference in the Boiler subsystem is the necessity to track and switch between multiple modes of calculation.

6.1.1.1 Boiling

The change in mass of the liquid CV can be calculated using Eq. (6.1).

$$\dot{m}_L = \dot{m}_{V,in} + \dot{m}_{V2L} - \dot{m}_{L2V} \tag{6.1}$$

Eq. (6.1) can be integrated to find the total mass of the liquid CV, m_L. For the liquid CV, the two modes of calculation are the heating mode and the boiling mode. While in the heating mode, the liquid CV absorbs heat from the metal and changes temperature accordingly. The UFEE can be arranged as presented in Eq. (6.2).

$$m_L C_L \dot{T}_L = \dot{m}_{L,in}(h_{L,in} - h_{f,L}) - \dot{m}_{L2V}(h_{g,L} - h_{f,L}) + \dot{m}_{V2L}(h_{f,V} - h_{f,L}) + \dot{Q}_{M2L} - \dot{Q}_{L2V} \tag{6.2}$$

The heating mode is in effect when the temperature of the liquid is below the saturation temperature at the current pressure. In this state, the mass flow due to evaporation, $\dot{m}_{L2V}$, is assumed to be zero. The calculation can be performed using Eq. (6.3).

$$\dot{T}_L = \frac{\dot{m}_{L,in}(h_{L,in} - h_{f,L}) + \dot{m}_{V2L}(h_{f,V} - h_{f,L}) + \dot{Q}_{M2L} - \dot{Q}_{L2V}}{m_L C_L} \tag{6.3}$$

In theory, the boiling mode is achieved when the temperature of the liquid CV is equal to the saturation temperature at the current pressure. Due to numerical error, it is necessary to consider an acceptable range where saturation can be assumed, i.e. $|T_L - T_{sat}(P_v)| \leq \varepsilon$. As previously

mentioned, the temperature of the liquid CV can be assumed constant while in the boiling mode, i.e. $\dot{T}_L = 0$. Therefore, Eq. (6.2) can be rearranged to calculated the boiling mass flow as seen in Eq. (6.4).

$$\dot{m}_{L2V} = \frac{\dot{m}_{L,in}(h_{L,in} - h_{f,L}) + \dot{m}_{V2L}(h_{f,V} - h_{f,L}) + \dot{Q}_{M2L} - \dot{Q}_{L2V}}{h_{g,L} - h_{f,L}} \tag{6.4}$$

It should be noted that the liquid-vapor interface is quite large within the drum of the boiler. For this reason, it is necessary to consider a convective heat transfer, $\dot{Q}_{L2V}$, between the boiler liquid and vapor CVs. This heat transfer can be represented by Eq. (6.5).

$$\dot{Q}_{L2V} = H_{L2V}A_{L2V}(T_L - T_V) \tag{6.5}$$

In this model, the mass flow into the liquid CV, $\dot{m}_{L,in}$, is calculated by a PID control block regulating water level. At steady state, this mass flow settles to be approximately equal to the boiling mass flow, $\dot{m}_{L2V}$.

6.1.1.2 Condensation

In reality, phase change within a boiler is not simply a one way process. Abrupt pressure changes from valve openings and various other effects can cause the subsystem to temporarily enter a state where vapor would condense back to liquid. In order to create a more robust model, it is imperative to include this phenomenon. As was necessary for the evaporation scenario, a switching mechanism can be employed to track and calculate values for two different states of the vapor CV: pressurization and condensation.

The change in mass of the vapor CV can be calculated using Eq. (6.6).

$$\dot{m}_V = \dot{m}_{L2V} - \dot{m}_{V2L} - \dot{m}_{V,out} \tag{6.6}$$

Eq. (6.6) can be integrated to find the total mass of the vapor CV, m_V. For the vapor CV, the UFEE can be arranged as presented in Eq. (6.7).

$$m_V C_V \dot{T}_V = \dot{m}_{L2V}(h_{g,L} - u_{g,V}) - \dot{m}_{V2L}(h_{f,V} - u_{g,V}) + \dot{m}_{V,out}(h_{V,out} - u_{g,V}) + \dot{Q}_{L2V} \qquad (6.7)$$

The pressurization mode is in effect when the pressure of the vapor is less than or equal to the saturation pressure of vapor at the current vapor temperature. In this state, the condensation mass flow, $\dot{m}_{V2L}$, is considered to be zero. The temperature of the vapor CV can be calculated by rearranging Eq. (6.7) into the form shown in Eq. (6.8)

$$\dot{T}_V = \frac{\dot{m}_{L2V}(h_{g,L} - u_{g,V}) + \dot{m}_{V,out}(h_{V,out} - u_{g,V}) + \dot{Q}_{L2V}}{m_V C_V} \qquad (6.8)$$

The condensation mode is in effect when the pressure of the vapor exceeds the saturation pressure at the current vapor temperature. In the condensation mode, the vapor temperature is considered to be constant, and thus the condensation mass flow can be calculated by rearranging Eq. (6.7) into the form displayed in Eq. (6.9).

$$\dot{m}_{V2L} = \frac{\dot{m}_{L2V}(h_{g,L} - u_{g,V}) + \dot{m}_{V,out}(h_{V,out} - u_{g,V}) + \dot{Q}_{L2V}}{h_{f,V} - u_{g,V}} \qquad (6.9)$$

6.2 Redlich-Kwong Equation of State

Due to the presence of a vapor CV, it is necessary to calculate the pressure of the boiler subsystem, as was done for the superheater in Chapter 5. The high pressure and high temperatures observed in the boiler point once again to the RK equation, shown here in Eq. (6.10), [13].

$$P_V = \frac{RT_V}{v - b} - \frac{a}{\sqrt{T_V} v (v + b)} \qquad (6.10)$$

28

It should be noted that for regions of low volatility for the HRSG, the a boiler model should predict pressure to be at the current saturation pressure for the given vapor temperature. It was for this reason that previous boiler models assumed the pressure within the boiler to follow the saturation pressure exactly, [1]. Although this produces a lower computational burden, such a model is not robust to significant perturbations and fails to capture the true behavior of higher energy systems such as the HP system. On the contrary, the use of the RK equation allows the boiler subsystem to settle naturally to saturation conditions while remaining robust in more volatile transient simulation.

6.2.1   Volume Calculation

A key difference in the boiler calculations is the presence of two separate CVs which share the total volume of the subsystem. This requires an indirect calculation of the vapor specific volume for use in Eq. (6.10). First, the volume of the liquid must be calculated using Eq. (6.11).

$$V_L = \frac{m_L}{\rho_L} \tag{6.11}$$

The vapor volume can then be calculated by a subtraction from the total volume of the boiler subsystem, as shown in Eq. (6.12).

$$V_V = V_{total} - V_L \tag{6.12}$$

The molar specific volume can be calculated by dividing the vapor volume by the total moles of steam within the boiler, demonstrated by Eq. (6.13)

$$v = \frac{V_V}{N_V} \tag{6.13}$$

$$N_V = \frac{m_V}{M_w} \tag{6.14}$$

In Eq. (6.14), M_w represents the molar mass of water.

6.3   Volumetric Energy Contribution

In the early stages of developing a robust boiler model, a notable issue observed among the simulation results was a significant temperature separation between the liquid and vapor CV's of the boiler. This phenomenon, although theoretically possible for short periods of time, is not realistic as the contents of a boiler will sustain near saturation conditions during the majority of operation. In an effort to remedy this inaccuracy, attention was given to the consideration of a real gas within the boiler. In non-ideal pressure and temperature conditions, the $\frac{d(mu)}{dt}$ term of the UFEE (Eq. (5.3)) can no longer be approximated as $m_V C_V \dot{T}_V$, but instead must include a secondary term associated with a change in energy due to a change in volume. The Redlich-Kwong pressure equation allows this term to be solved for through direct differentiation. A detailed derivation of this term is presented in Appendix B. The additional change in volume term is presented in Eqs. (6.15) and (6.16).

$$\frac{d(mu)}{dt} = \dot{m}_V u_{g,V} + m_V C_V \dot{T}_V + m_V Z \qquad (6.15)$$

$$Z = \frac{1.5a}{(v+b)\sqrt{T_V}} \left(\frac{\dot{m}_{L2V} - \dot{m}_{V2L} - \dot{m}_{out}}{M_w} \right) \qquad (6.16)$$

Z represents the volume change contribution to the change in internal energy. This adjustment was made to the solving of Eq. (6.7) when calculating the instantaneous change in temperature.

Upon implementation it was noted that this realistic addition to the temperature calculation had a negligible effect on the results of the simulation during regular operation. Furthermore, the adjustment did not solve the issue of temperature separation. In hindsight, this is a somewhat expected result, as the addition of the volumetric term is inherently transient. Adjusting the rate of change of temperature should not have a significant effect on the steady state equilibrium of

the system, but it should merely adjust the path by which the system approaches equilibrium. Ultimately, the volumetric term does theoretically make the temperature change calculation more robust to abrupt changes in the system, and the added computational load is quite small, so, for the purposes of this research, the volumetric adjustment was left in the model.

6.4   Evaporative Cooling

In previous sections regarding the liquid CV of the boiler, two conditions have been considered: liquid water below saturation temperature and liquid water at (or near) saturation temperature. These conditions have been properly accounted for through the use of the switching mechanism. Naturally, a third condition must be considered, namely liquid water above saturation temperature. This condition in reality is unstable, as water above saturation temperature would evaporate to approach a new equilibrium. This natural evaporation has a cooling effect on the liquid CV as the phase change takes energy from the liquid. It should be noted that, unlike the previous two conditions, this evaporative cooling mode suggests that both a temperature change and a mass transfer will occur simultaneously. A switching mechanism cannot properly approximate the mass flow as the temperature can no longer be assumed to be constant. To remedy this imbalance of variables to equations, it is necessary to take a step back from the lumped CV assumption and analyze the macro and micro-scale conditions of a boiler, specifically at the interface of the liquid and the vapor. Macro-scale conditions of a liquid and vapor may present non-saturation conditions. However, it is reasonable to assume that the micro-scale conditions of the liquid/vapor interface will be held at saturation. Without a detailed finite element model of the liquid/vapor interface, assumptions must be made about the conditions of this mass exchange. For the purpose of this model, it is both reasonable and convenient to assume the mass transfer of this evaporative cooling mode to be that of the liquid CV boiling with the previous temperature of the CV taken to be the

31

current saturation condition. This assumption takes advantage of the fact that on a microscale, the temperature of the liquid currently evaporating will be held constant. This mass flow, although not entirely accurate, adequately captures the behavior of the evaporative cooling phenomenon, and thus, pushes the system to the proper equilibrium.

6.4.1 Mass Flow Correction Factor

Given the mass flow assumption, an attempt was made to increase the accuracy of the evaporative cooling mass flow. The process is pressure driven; therefore, a simple pressure difference correction factor was added to the mass flow, presented in Eq. (6.17).

$$\dot{m}_{L2V} = \dot{m}_{L2V_{sat}} + k_{ec}(P_{sat} - P_V) \tag{6.17}$$

In Eq. (6.17), k_{ec} represents a tunable constant that can be adjusted to allow more or less evaporation mass flow in the evaporative cooling mode. It was observed upon implementation that changing this constant had a somewhat negligible effect on the system, as the system would always approach the same total mass flow by adjusting $\dot{m}_{L2V_{sat}}$ accordingly. This resistance to change in the system was observed in many aspects regarding tunable parameters.

CHAPTER 7: VALIDATION AND SIMULATION

7.1   Full Load Start-Up

A major milestone of this research focused on producing a transient model that would show physically realistic behavior and reach steady state values comparable to those provided by Siemens Energy Inc. for the reference HRSG running at full power output. It is the philosophy of this research that one should not produce a model with the intentions of matching the provided data exactly. Instead, developing an accurate model of the physical phenomena present in an HRSG should in turn produce results accurate to reality. At the same time, this mindset produces a versatile model that will respond accurately to perturbation and alternative input conditions. The results displayed below show a transient simulation of the presented HRSG model from start-up to full capacity.

Two coupled factors play into the transient behavior of the pressure within an HRSG: physical location and energy magnitude. The HP system is the closest system to the inlet of the flue gas, followed by the IP, and later the LP system. This suggest that the HP system will respond to a change in the flue gas temperature first, and it will continue to receive the most energy throughout the start-up of the HRSG. Figure 7.1 shows the start-up simulation results for the pressure in each pressure system. As expected, the HP system pressurizes first and reaches the highest pressure of the three systems. The IP system pressurizes second and reaches a lower steady state pressure than the HP system. Finally, the LP system pressurizes last and reaches the lowest steady state value of the three systems.
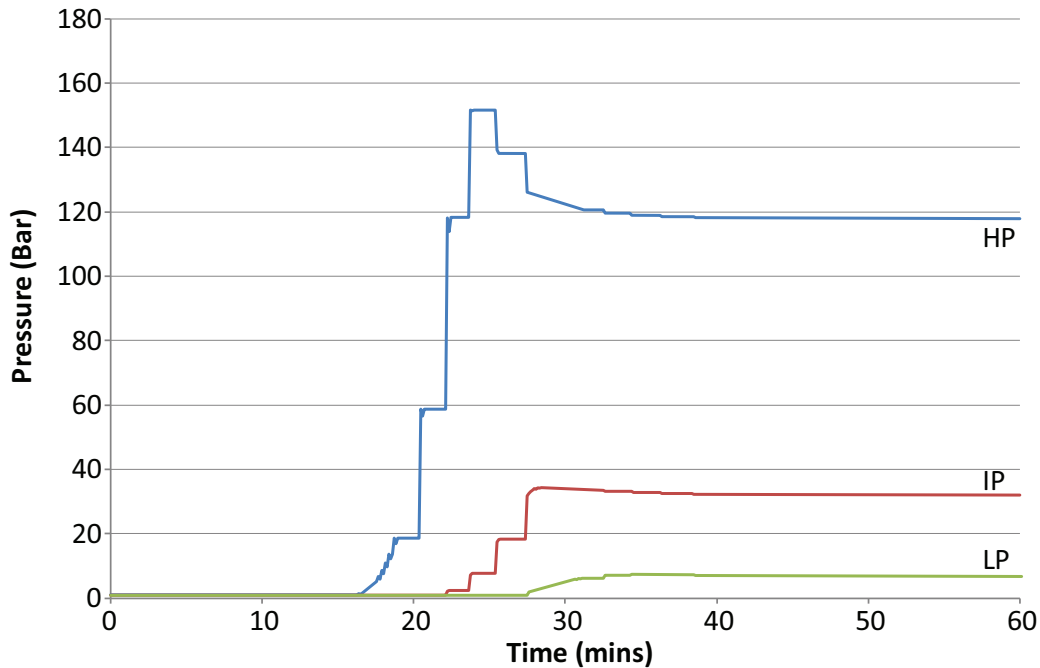
Figure 7.1: SIMULATED PRESSURES OF THREE STAGE HSRG

The jagged transient trends seen in Figure 7.1 and the following graphs are not a result of simulation fidelity, but are instead an after effect of T3000's data archiving. This phenomenon will be discussed in detail in Chapter 8.

Table 7.1 shows a comparison of the steady state pressure values reached in this transient simulation with those provided by Siemens for the reference HRSG. All three systems reached values within 2 bar of the reference data.

Table 7.1: COMPARISON OF PRESSURE DATA WITH SIMULATION.

	T3000 Simulation	Siemens Data
HP	117.77 bar	118.12 bar
IP	32.11 bar	30.24 bar
LP	5.35 bar	6.82 bar

Although a small amount of pressurization can be attributed directly to an increase in temperature, the most significant contribution to pressure increase is boiling. It follows that the onset of this mass flow should correspond to a significant increase in the pressure within each pressure system.

In Figure 7.2, the exact timing of mass flow initiation is slightly skewed by the erroneous constant value phenomenon. That being said, the beginning of boiling within each pressure system lines up quite accurately with the initial pressure increases shown in Figure 7.1.

The mass flow trends shown in Figure 7.2 present an insightful visual representation of the switching mechanism discussed in Chapter 6. The mass flow begins at zero, as the system is not currently at saturation conditions. This trend continues until saturation is reached, at which point the switch is flipped and mass flow is produced at constant temperature.
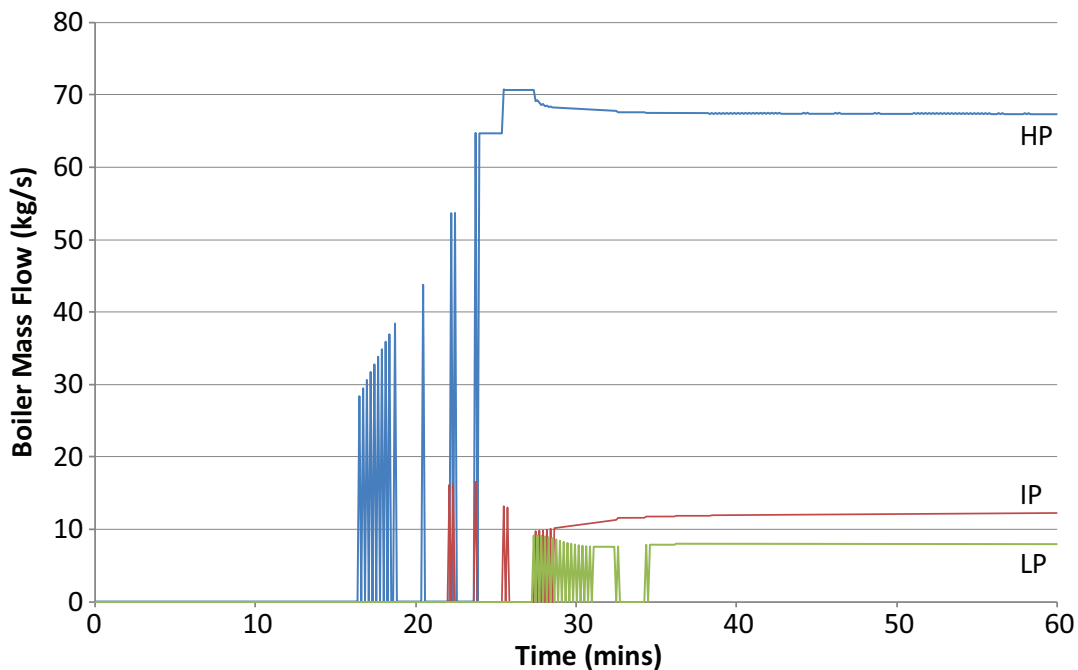
Figure 7.2: BOILER FLOW RATES AT THREE STAGES

Table 7.2: COMPARISON OF MASS FLOW DATA WITH SIMULATION.

	T3000 Simulation	Siemens Data
HP	67.19 kg/s	66.16 kg/s
IP	12.45 kg/s	11.83 kg/s
LP	7.88 kg/s	8.21 kg/s

This mass flow is initially unstable. Introducing more mass to the vapor CV raises the pressure of the system, and with it, the saturation temperature needed for boiling. The system switches back to the heating mode and repeats this process for some time. As the system approaches steady state, the boiling mode becomes more stable until a state of continuous boiling is reached with slight adjustments from the evaporative cooling mode to settle at the steady state value. This chain of events is observed in all three pressure systems.

The steady state values for the boiler mass flow of each pressure system is presented in Table 7.2. Once again, the values for the full capacity simulation accurately approximate the data for the reference HRSG.
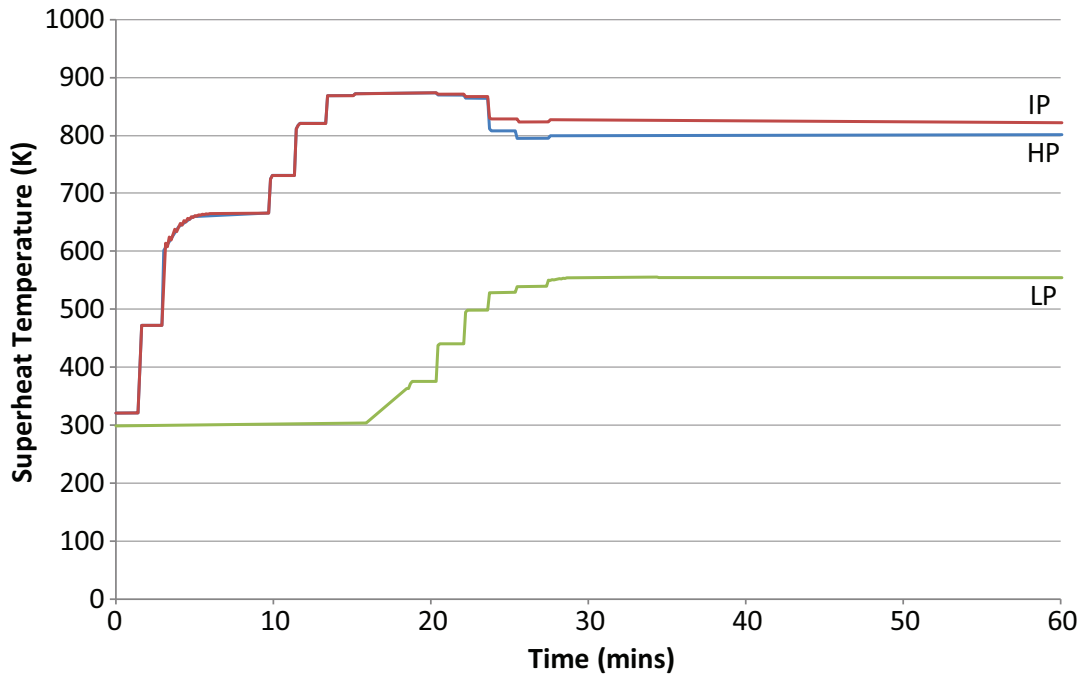
Figure 7.3: TEMPERATURES OF SUPERHEATED STEAM

Figure 7.3 shows the transient temperature trends of the final superheater within each pressure system. For the IP system, this refers to the second reheater. The final HP superheater and the second reheater are both located in Cluster 1, the cluster closest to the inlet of the flue gas. It follows that these two subsystems will have similar temperature trends and closely follow the input flue gas ramp-up profile. The contents of Cluster 1 should react immediately to the introduction of the hot flue gas. The LP superheater, located in Cluster 4 will reach a much lower temperature as the flue gas interacting with later clusters will have lost a significant amount of heat to the previous clusters. The response time of the LP system will also be delayed as more heat will be initially taken by the previous clusters. These expected responses are observed in Figure 7.3.

Table 7.3: COMPARISON OF SUPERHEAT DATA WITH SIMULATION.

	T3000 Simulation	Siemens Data
HP	801.49 K	840.43 K
IP	822.26 K	839.15 K
LP	553.82 K	520.93 K

A comparison of the steady state values for the final superheater temperature of each pressure system is presented in Table 7.3. A noticeable error is apparent for the superheater temperatures predicted by the model. It is believed that these discrepancies can be reduced through further tuning of heat transfer coefficients and other system parameters, but as previously mentioned, the goal of this research focuses on producing accurate behavior over steady state results. As an added difficulty, significant tuning of system parameters can lead to numerical oscillation unless the sample time of the simulation is appropriately decreased. For the purposes of this research, the steady state values given in Table 7.3 have been deemed acceptable.

7.2   Partial Load Start-Up

It has been demonstrated that the model shows good agreement and realistic behavior for the full capacity case. However, in reality, most power plant start-ups will not immediately ramp up to full capacity. This practice would strain the system and fatigue the material exposed to the flue gas. It is important to allow all parts of the HRSG system to reach an increased temperature before proceeding to higher load capacities. For this reason, the model will be compared with transient data provided by Siemens for a partial load ramp-up. To simulate this on the HRSG model, the GT exhaust temperature and mass flow profiles provided by Siemens for the partial capacity ramp-up have replaced the respective profiles associated with full capacity case. The initial values of the the simulation have also been adjusted to match those shown in the reference data. When an HRSG is powered down, it takes a significant amount of time for all parts of the system to reach equilibrium with atmospheric conditions. For this particular set of start-up trends, many initial temperatures are much higher than 298 K.
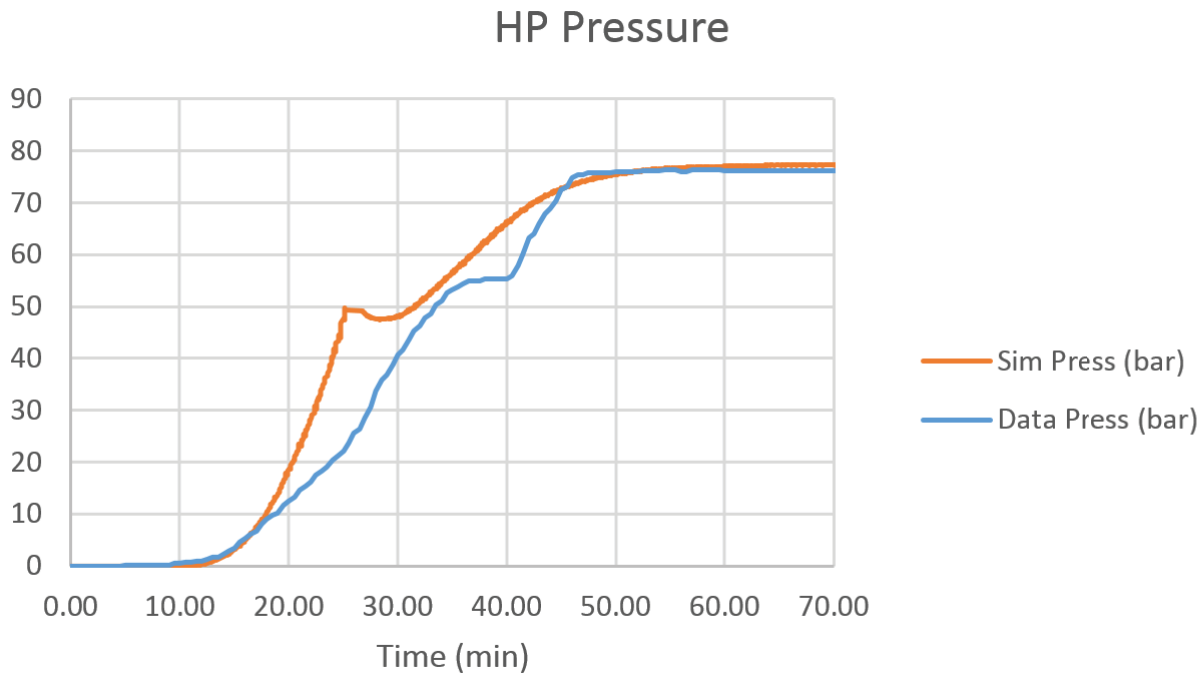
Figure 7.4: ANALYSIS OF HP PRESSURE

Figure 7.4 compares the simulated HP pressure trend with that of the reference HRSG. The initiation of pressurization predicted by the simulation is in good agreement with reference trend. Although the model appears to pressurize at a faster rate than the reference HRSG, the general behavior of the simulated trend adequately mimics the reference data. A significant feature is the relatively constant pressure region seen at approximately 25 to 30 minutes for the simulated trend and 35 to 40 minutes for the reference data trend. This region is indicative of the valve opening described in Chapter 5. Considering the tunable parameters associated with this valve opening, it is possible to optimize the timing and maximum k_f value to better match this reference trend.
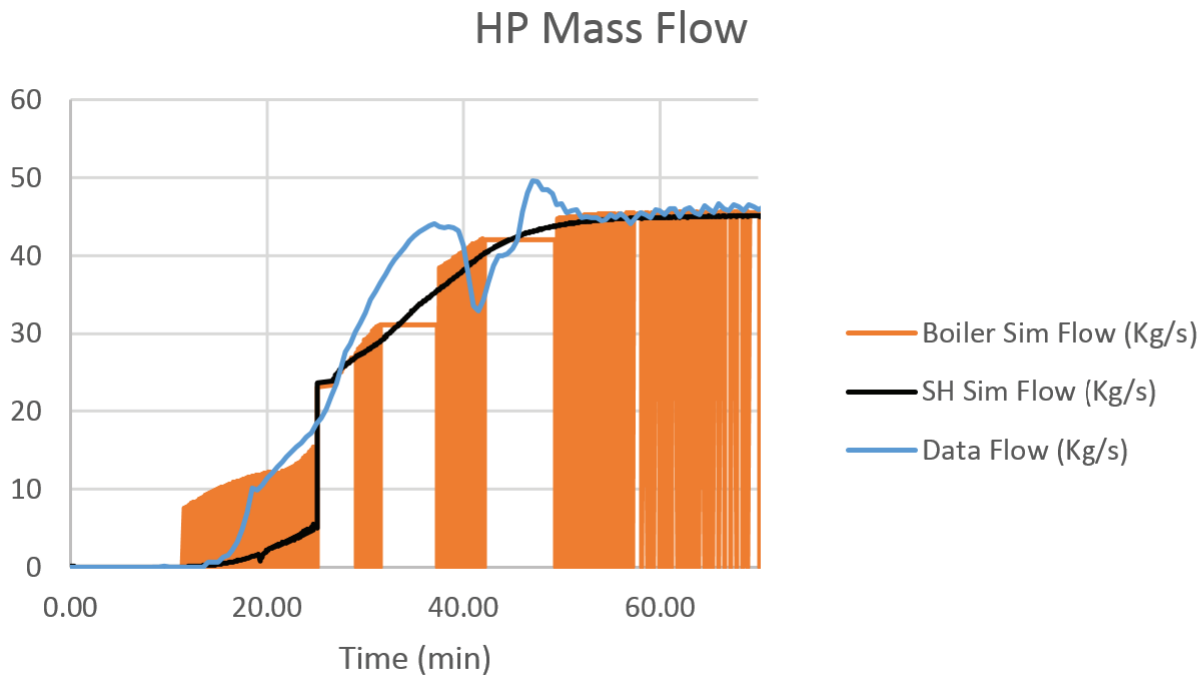
Figure 7.5: ANALYSIS OF HP MASS FLOW

Figure 7.5 shows three trends. The blue trend represents the exhaust flow of the HP system as described by the reference data. The orange trend represents the simulated mass flow from liquid to vapor in the HP boiler. As was observed in the full capacity start-up case, this boiler mass flow is driven by the switching mechanism described in Chapter 6. Boiler mass flow is not present until saturation conditions are reached. Mass flow then switches on and off until leveling out at steady state. The black trend represents the mass flow exiting the final superheater of the simulated HP system. This mass flow is the best comparison to the exhaust mass flow provided by the data. The superheater mass flow is held to a low value while the valve is in the closed condition. The initiation of the valve opening can be observed as a vertical jump in the superheater mass flow trend. Given that both the boiler and superheater trends (as well as every other simulated trend for the partial capacity start-up case) display a vertical jump followed by a short region of constant

value at this time, it is apparent that this swiftly changing region of the simulation has been skewed by a graphical archiving error. For reasons explained in detail in Chapter 8, this region can be assumed to be a smooth interpolation for both mass flow trends.

The reference data depicts a region of significant oscillation. This oscillation coincides with the real timing of the valve opening as described by the pressure trend in Figure 7.4. The real trend is not exactly mimicked by the model. The valve control of the real HRSG is a closed loop control dynamically adjusting the pressure profile of the system. For the model, the valve control is an open loop control and thus does not dynamically adjust once initiated. Keeping this in mind, the simulated superheater mass flow appears to follow the general trend the reference mass flow adequately.
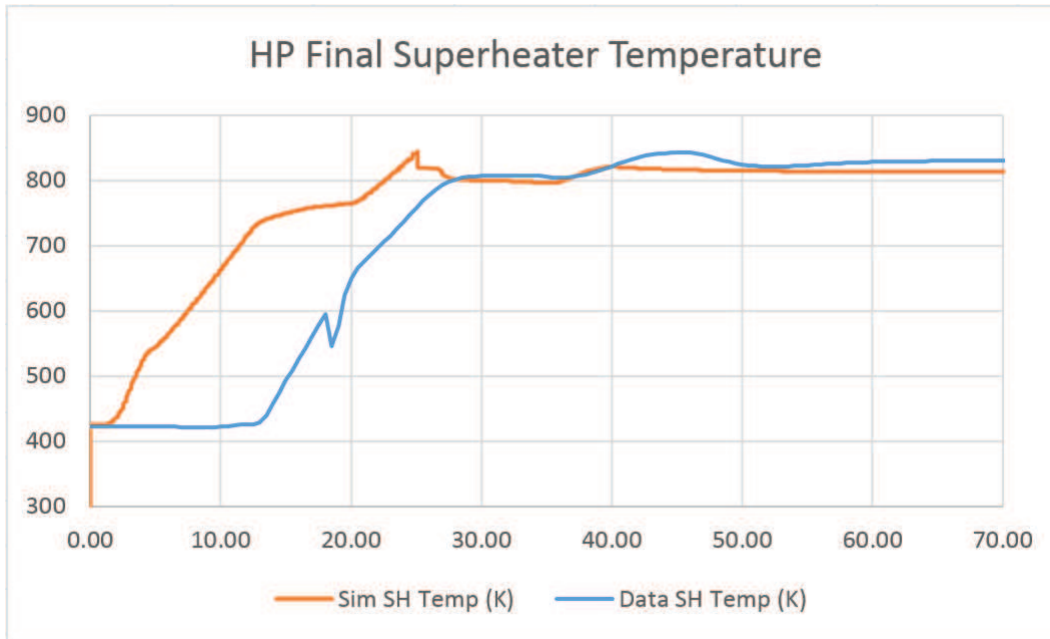
Figure 7.6: ANALYSIS OF HP FINAL SUPERHEATER TEMPERATURE

The HP final superheater temperature, displayed in Figure 7.6, does reach a similar steady state temperature as is depicted by the reference data. However, it is apparent that the simulation responds much faster to the introduction hot flue gas. This discrepancy is a result of the method of temperature monitoring used on the reference HRSG. It is observed that the real superheater temperature does not increase until mass flow has begun in the HP system. This implies that the thermal couple does not reside within the superheater subsystem itself, but instead beyond the subsystem, perhaps passed a valve. This insight suggests that the provided superheater temperature data does not properly account for the increasing temperature of stagnant steam within the superheater pipes at start-up. With this in mind, the behavior of the simulated superheater is expected.
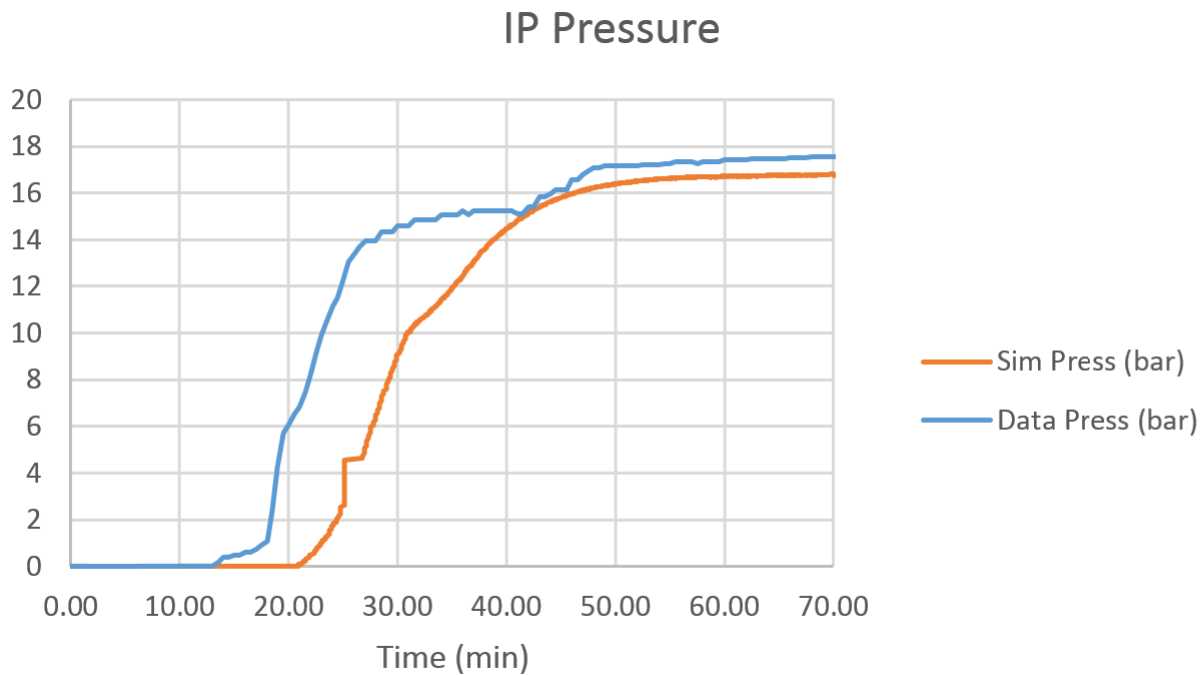
Figure 7.7: ANALYSIS OF IP PRESSURE

Figure 7.7 shows a comparison of the simulated pressure trend with the reference data for the IP system. The general behavior of the simulation shows good agreement with the behavior of the reference HRSG. That being said, there appears to be an approximately 5 minute lag in the IP system simulation when compared to the reference data. This timing discrepancy, though significant, can be adjusted through further optimization of tunable parameters in the model. The valve opening for the IP system appears to occur just after the 40th minute of the start-up ramp. The simulated valve opening appears to have a less significant effect on the simulated IP pressure trend, but a small inflection can be observed after the 30th minute of simulated time. This once again shows a room for improvement in regards to the timing of valve opening, but the overall behavior of the IP system is adequately captured by the model.
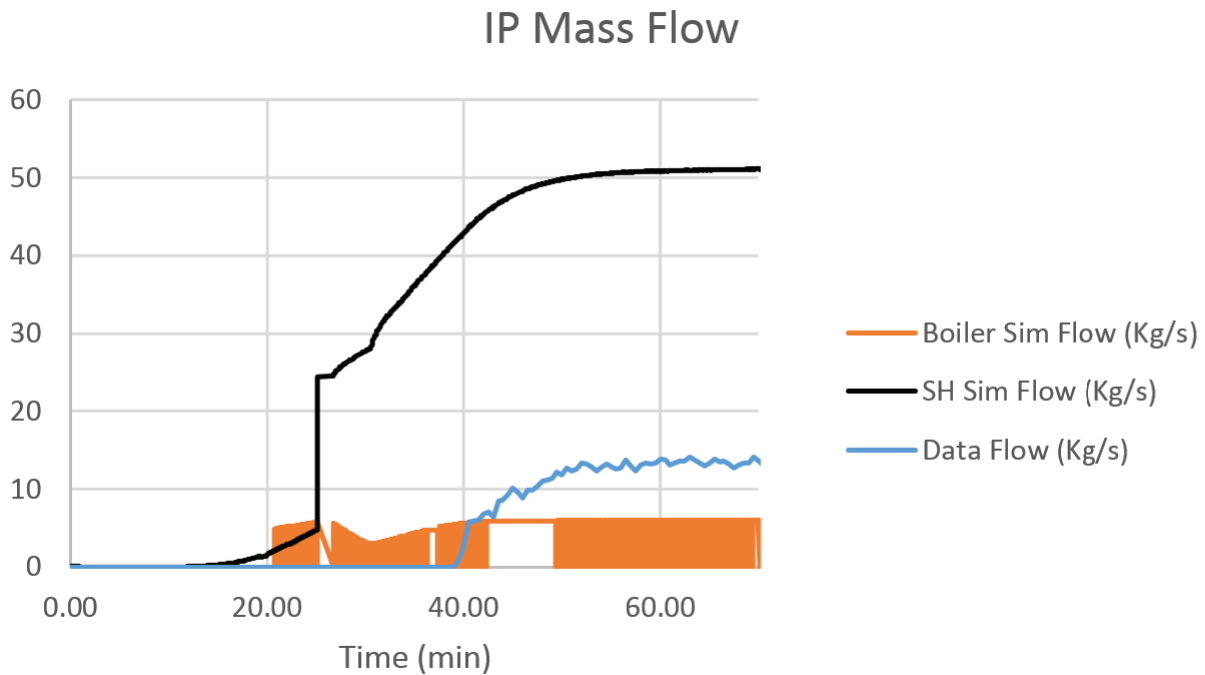
Figure 7.8: ANALYSIS OF IP MASS FLOW

Figure 7.8 presents the mass flow trends associated with the IP system, as were presented in Figure 7.5 for the HP system. A key difference in the IP system is the inclusion of the Cold Reheat Mixing. This mixing adds a significant amount of mass flow to the IP system before entering the final superheaters. For this reason, and a lack of knowledge in regards to the exact placement of the mass flow sensor within the IP system, it is difficult to draw insight from a direct comparison to the discrete subsystems of the IP model. Furthermore, it can be observed that the timing of the initial mass flow as suggested by the data is significantly later that the initial pressurization. This implies that a different logic is employed for valve control when compared to the HP system.

It can be said that the behavior depicted by the simulated trends is realistic in that it behaves much like the HP system. The IP exhaust flow predicted by the model is strongly coupled with the

HP flow as the HP exhaust is directly contributing to the Cold Reheat Mixing. This produces a superposition of the behaviors seen in the HP and IP systems.

Figure 7.9 presents a comparison of the LP simulated pressure trend to the data from the reference HRSG. It is important to note the scale of the values observed in the LP system when comparing with the trends from the HP and IP system. With that in mind, the initial and steady state errors of the LP model are quite negligible. The timing of the simulated pressurization appears to be leading the real data by approximately 10 minutes on average. Once again, this timing discrepancy can be remedied through system optimization. The over all behavior of the LP pressure trend appears to reasonably comparable to that of the real HRSG.
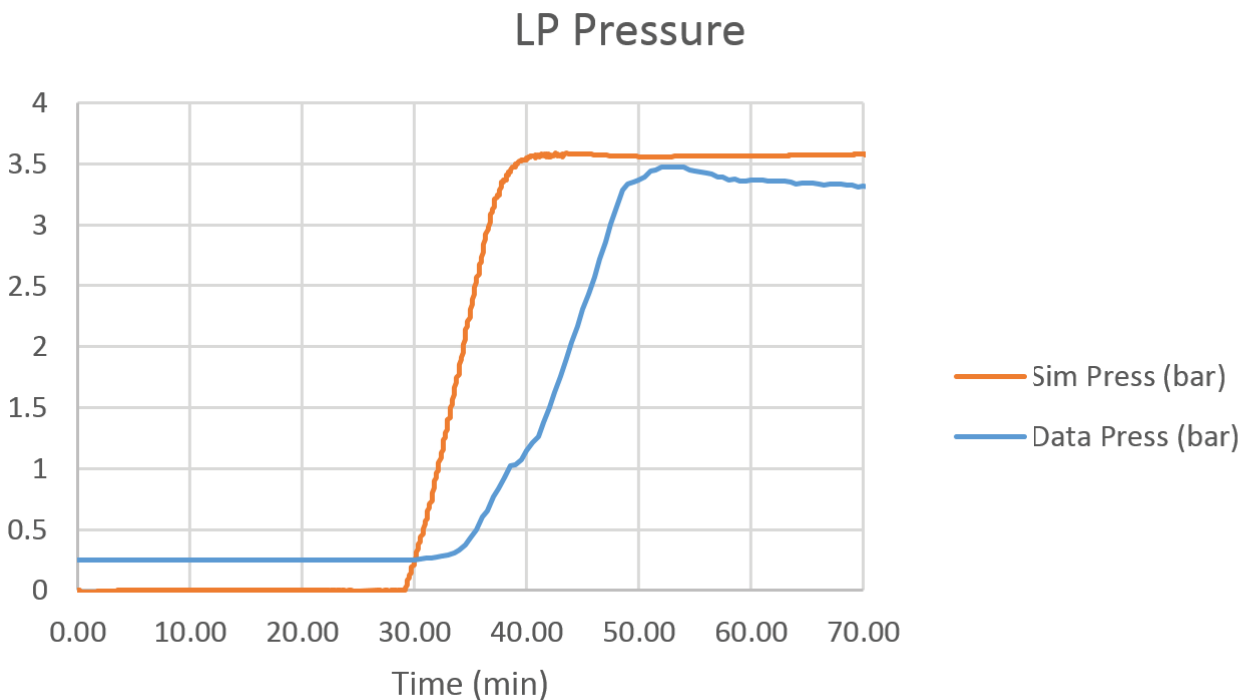
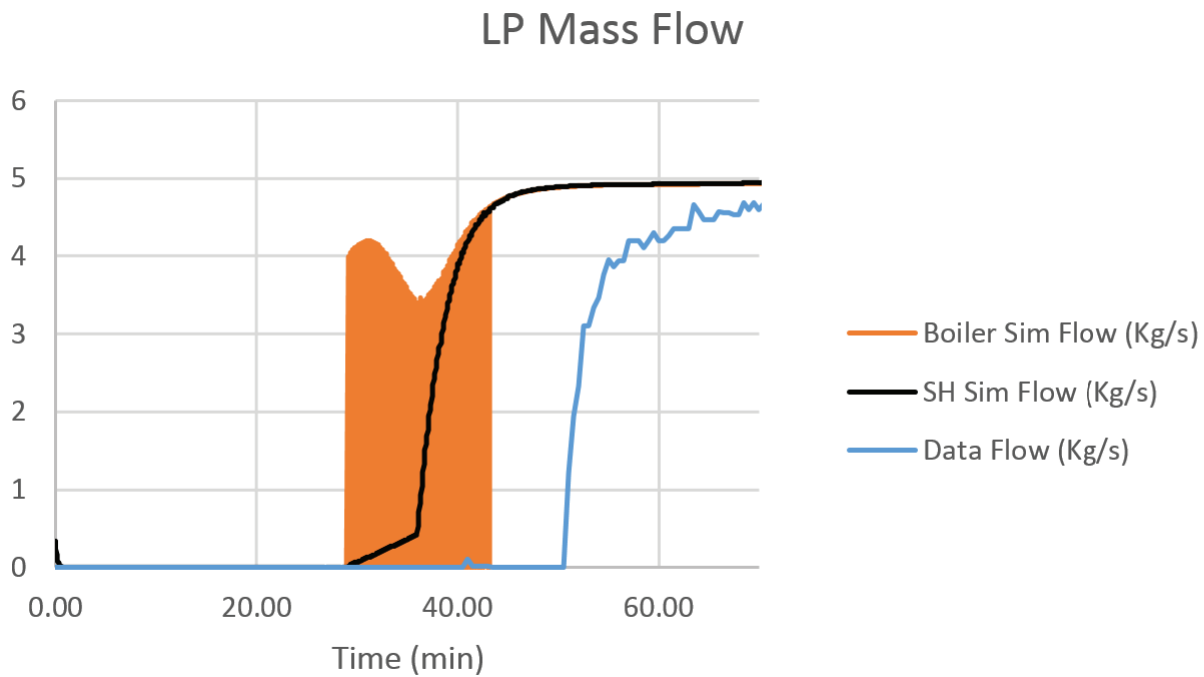

Figure 7.9: ANALYSIS OF LP PRESSURE

Figure 7.10:   ANALYSIS OF LP MASS FLOW

Figure 7.10 presents the various mass flow trends associated with the LP system. Here the simulation once again appears to lead the real data by a significant margin. It is interesting to note that the mass flow of the real LP system does not begin simultaneously with the initial increase in pressure. This can be explained by the dual nature of pressure increase for a gaseous CV. The pressure of a CV can increase due to the introduction of more mass or naturally from an increase in temperature. The latter case is not very significant for the HP and IP systems, as the pressure increase due to mass flow is orders of magnitude larger. The lower pressure levels seen in the LP system allow for this natural pressurization to play a larger role.

CHAPTER 8: MODELING CHALLENGES

8.1   Computation Speed vs. Numerical Accuracy

It is a major goal of this research to produce a model that is both accurate and easy to simulate. Obviously, higher fidelity models will produce more accurate results. This research focuses on developing a low complexity model, through the use of lumped CVs, that will still provide insightful predictions for the transient behavior of an HRSG system. Along with the amount of CV calculations, the sample rate of the simulation plays a large role in the accuracy of transient behavior. Lack of powerful computational resources placed a limitation on the speed of simulation available for this research. For this reason, the time used in calculations within the simulation has been dilated to 5 times real time. By spreading out the time of simulation, the fidelity of the model can be increased. Upon analysis of results, this time dilation can be accounted for to produce pseudo real time trends.

Through cooperation with Siemens, the LP model developed by Caesar, [1], has been shown to produce valid real time simulation when run on a more powerful computer. With more computational power, a smaller sample rate can be used, and the time dilation can be removed. Although the model presented in this document is significantly larger and more complex, it is believed that real time simulation is feasible with increased computational power.

8.2   Numerical Oscillations

Numerical oscillations provide a roadblock for removal of time dilation and significant tuning of the HRSG model. When the rates of change of system parameters are remarkably high, discrete

simulations tend to overshoot the true trend of said parameter. In some cases, this overshoot can lead to significant oscillation as the system attempts to stabilize itself. Ignoring cases of incorrect simulation setup, these oscillations tend to settle to a steady state value as the input flue gas temperature reaches a steady state of its own. This natural tendency of the system to approach steady state is a testament to the robustness of the simulation. That being said, the regions of significant oscillation are of no use for analyzing the behavior of transient trends, as these oscillations are a result of computational inaccuracy, and are not indicative of real physical phenomena. For this reason, it is necessary to properly assess the ability of the computational system the model is being run on and dilate time appropriately. It is also important to keep oscillation in mind when tuning the system. This is especially true for vapor CVs like the superheaters, as the thermal inertia of water vapor is quite low compared to liquid water. It has been observed that heat transfer coefficients, though very flexible, must not be increase too significantly in an attempt to achieve more accurate steady state values. A threshold exists where temperature oscillation will occur during start-up.

8.3   Erroneous Constant Values

One significant challenge faced during the development of this model was a graphical error producing significant regions of constant values on the archived T3000 trends, shown in Figure 8.1. T3000, as previously mentioned, is a plant monitoring software designed for use on control panels of power plants. By pushing the limits of this software, and creating the enormous flowchart diagram needed to model every aspect of a multi-pressure HRSG, a significantly large selection of values needed to be archived at any given time. This notion, coupled with the idea that this research was performed with a single computer, meant that the graphs outputted by T3000 were often overloaded.
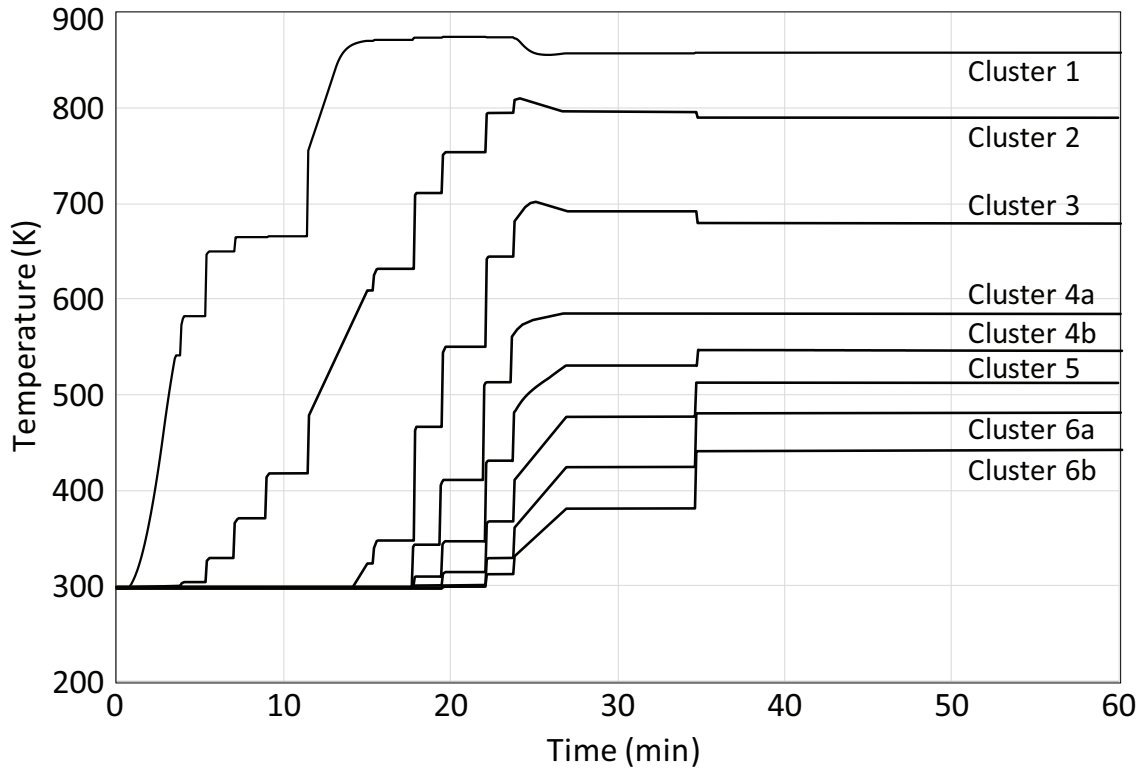
Figure 8.1: FLUE GAS TEMPERATURES ACROSS CLUSTERS

After thorough investigation into this issue, it was observed that this constant value phenomenon was solely in the archiving process of T3000. When the graphs of archive data were constant, the transient data being calculated by the model was unaffected and would continue to fluctuate as expected. It was discovered that a regular clearing of the archive data would temporarily avoid future erroneous constant values, and thus the validation graphs presented in the latter portion of this thesis show much smoother curves. For those plots where erroneous constant values are present, a smooth interpolation of data can be assumed.

CHAPTER 9: CONCLUSION

9.1 Research Overview

A theoretical model of a multi-pressure HRSG has been presented using a CV based approach to simulate individual subsystems as well as their geometric clustering. It has been shown that this theoretical model can be practically executed on Siemens Energy Inc.'s T3000 plant monitoring software. This transient simulation can be run at near real time with physically accurate behavior showing good agreement with the transient and steady state data provided by Siemens for a reference HRSG.

Furthermore, it has been shown that a switching mechanism can be implemented to accurately approximate the phase change phenomena within a boiler, specifically boiling and back-flow condensation. This back-flow condensation has been observed to effectively remove numerical inaccuracy associated with unnatural temperature separation between boiler liquid and vapor CVs. The RK equation has been effectively implemented as a means of calculating pressure. This pressure calculation is robust to abrupt perturbations as it accounts for steam pressures deviating from the saturation regime. Calculation of real gas volumetric energy contribution to rate of temperature change has been demonstrated, and it has been observed to have a negligible effect on the results of model simulation within the regime of the provided reference data. An approximated evaporative cooling mass flow has been presented to combat pressures lower than saturation conditions. The combination of these mechanisms has been shown to behave in a physically accurate manor and yield reasonably accurate transient trends in comparison with reference data.

9.2 Future Research

While the research presented in this thesis meets the objective of thoroughly modeling an HRSG system, there is still room for improvement of the model. Further developments can also be made to gain insight on other aspects of a traditional powerplant. Some potential improvements are discussed below:

9.2.1 Model Optimization

Due to the focus of this research on realistic transient behavior, there are many instances where the system is not optimally tuned for the provided steady state results. The large collection of tunable parameters poses a daunting task to any person or group wishing to thoroughly optimize a system such as the presented HRSG model. For this reason, it may be possible to implement an optimization algorithm, such as a neural network, to tune the system for stronger correlation with the data. This optimization not only lies out of the scope of current research, but also implies a need for much greater computational power.

9.2.2 Closed Loop Valve Control

As mentioned in Chapter 7, the current valve control system within the model is an open loop control. The valve is closed until a pressure threshold is reached, at which point the valve is slowly opened following a first order response to a desired maximum value. Implementation of a closed loop control monitoring pressure would be more analogous to the system used in the reference HRSG. This adjustment would also improve the model predictions for perturbation scenarios, as the current valve model cannot dynamically close.

9.2.3   Steam Turbine and Condenser Models

The model presented in this research focus specifically on the HRSG section of a traditional power plant. In the case of the Cold Reheat Mixing, the effects of the HP steam turbine are approximated to allow for simple simulation. The accuracy of this model could be increased with the addition of a steam turbine model, as the system would react to the dynamic response of turbine in regards to temperature and pressure drop from one pressure system to the next.

One promising area of research will be the addition of a condenser model, which is currently under development. Such a model, coupled with a steam turbine model, will essentially complete the cycle of the HRSG system, as the exhaust steam will be condensed and sent back to the LP economizer for preheating. This condenser model will use similar lumped CV methods to simulate the energy transfer from exhaust steam to a cooling medium at low pressures.

9.2.4   Boiler Swell/Shrink

Boiler swell/shrink is a significant interest of future development to the current boiler model. The presence of vapor bubbles within the riser tubes of the boiler subsystem pose a rather complex controls problem when attempting to predict the water level inside the boiler drum. Thermodynamic predictions of boiler water level are only accurate after the water reaches a new equilibrium and are actually contrary to the behavior of the water level during transients. For this reason, a predictive model of boiler water level would prove to be quite insightful into this phenomenon. It would also be possible to use such a model in plant monitoring software to effectively counter the swell/shrink effect and keep the HRSG running efficiently.

APPENDIX A: PIPE FLOW CONSTANT DERIVATION

For a simple pipe model, the head loss through a pipe can be described by Eq. (A.1),

$$h_f = \frac{fL\dot{X}^2}{2dg},$$ (A.1)

where f is a friction factor, L is the length, d is the diameter, $\dot{X}$ is the fluid flow velocity, and g is the acceleration due to gravity, [14]. The head loss can also be expressed as a function of the differences in pressure as shown in Eq. (A.2).

$$h_f = \frac{\Delta P}{\rho g}$$ (A.2)

Eqs. (A.1) and (A.2) can be set equal to each other as demonstrated in Eq. (A.3).

$$\frac{\Delta P}{\rho g} = \frac{fL\dot{X}^2}{2dg}$$ (A.3)

Note here that the g terms on each side of Eq. (A.3) cancel out.

It is known that velocity can be represented in the form displayed in Eq. (A.4).

$$\dot{X} = \frac{\dot{m}}{\rho A}$$ (A.4)

This velocity equation can be substituted into Eq. (A.3) to yield Eq. (A.5).

$$\frac{\Delta P}{\rho} = \frac{fL\dot{m}^2}{2d\rho^2 A^2}$$ (A.5)

Isolating $\dot{m}$ will produce Eq. (A.6).

$$\dot{m}^2 = \rho \Delta P \frac{2dA^2}{fL}$$ (A.6)

By taking the square root of each side, an equation in similar form to that of Eq. (5.17) can be achieved, as shown in Eq. (A.7).

$$\dot{m} = \sqrt{\frac{2dA^2}{fL}} \sqrt{\rho} \sqrt{\Delta P} \tag{A.7}$$

Due to the complex geometric conditions observed within an HRSG, it is convenient to approximate $\sqrt{\frac{2dA^2}{fL}}$ as one combined parameter, and thus k_f can be defined by Eq. (A.8).

$$k_f = \sqrt{\frac{2dA^2}{fL}} \tag{A.8}$$

For the purposes of this research, k_f is considered a tunable parameter, as it must be properly adjusted to adequately capture the complex geometric conditions of the HRSG.

APPENDIX B: VOLUMETRIC ENERGY CONTRIBUTION

DERIVATION

A change in internal energy can be considered a function of temperature and volume, as denoted in Eq. (B.1).

$$du = C_v dT + [T(\frac{\partial P}{\partial T})_V - P]dV \qquad (B.1)$$

If an ideal gas assumption is made, the pressure can be solved for using the ideal gas equation, shown in Eqs. (B.2) and (B.3).

$$PV = nRT \qquad (B.2)$$

$$P = \frac{nRT}{V} \qquad (B.3)$$

If Eq. (B.3) is plugged in to Eq. (B.1), it is observed that the term within the brackets is equal to zero, as presented in Eqs. (B.4) and (B.5).

$$(\frac{\partial P}{\partial T})_V = \frac{nR}{V} \qquad (B.4)$$

$$[T(\frac{\partial P}{\partial T})_V - P] = \frac{nRT}{V} - P = 0 \qquad (B.5)$$

This means for an ideal gas, this extra term does not have an effect on the transient of the system. However, for a case where the RK equation is used to calculate pressure, this term is not zero.

The RK equation for pressure calculation is shown in Eq. (B.6).

$$P = \frac{RT}{v - b} - \frac{a}{\sqrt{T}v(v + b)} \qquad (B.6)$$

A similar partial differentiation with respect to temperature can be perform on Eq. (B.6), as presented in Eq. (B.7).

$$\left(\frac{\partial P}{\partial T}\right)_V = \frac{R}{v-b} + \frac{a}{2T^{\frac{3}{2}}v(v+b)} \tag{B.7}$$

Eq. (B.7) can be applied to Eq. (B.1) to solve for the effect of volume change on internal energy, seen in Eqs. (B.8) and (B.9).

$$\left[T\left(\frac{\partial P}{\partial T}\right)_V - P\right] = \frac{RT}{v-b} + \frac{a}{2\sqrt{T}v(v+b)} - P = \frac{1.5a}{\sqrt{T}v(v+b)} \tag{B.8}$$

$$du = C_v dT + \frac{1.5a}{\sqrt{T}v(v+b)}dV \tag{B.9}$$

Dividing through by dt, Eq. (B.9) can be written in the form shown in Eq. (B.10).

$$\dot{u} = C_v \dot{T} + \frac{1.5a}{\sqrt{T}v(v+b)}\dot{V} \tag{B.10}$$

For the boiler subsystem presented in this document, the change in volume of the vapor CV, $\dot{V}_V$, is a function of the change in mass of the CV and the specific volume. This relation is presented in Eq. (B.11).

$$\dot{V}_V = \frac{v\dot{m}_V}{M_w} \tag{B.11}$$

In Eq. (B.11), $\dot{m}_V$ can be replaced by applying Eq. (6.6), shown in Eq. (B.12).

$$\dot{V}_V = \frac{v(\dot{m}_{L2V} - \dot{m}_{V2L} - \dot{m}_{V,out})}{M_w} \tag{B.12}$$

Eq. (B.12) can be applied to Eq. (B.10) to achieve the form seen in Eq. (6.15). This is displayed in Eq. (B.13)

$$\dot{u} = C_v \dot{T} + \frac{1.5a}{\sqrt{T}(v+b)} \left(\frac{\dot{m}_{L2V} - \dot{m}_{V2L} - \dot{m}_{V,out}}{M_w} \right) \tag{B.13}$$

LIST OF REFERENCES

[1] Caesar, A. M., 2018. "Thermodynamic Modeling and Transient Simulation of a Low-Pressure Heat Recovery Steam Generator Using Siemens T3000". MS Thesis, University of Central Florida, Orlando, FL.

[2] Erikson, V. L., ed., 2017. *Heat Recovery Steam Generator Technology*, 1 ed. Woodhead Publishing, Cambridge, MA, ch. 1, pp. 1–15.

[3] Tomar, G., Biswas, G., Sharma, A., and Agrawal, A., 2005. "Numerical simulation of bubble growth in film boiling using a coupled level-set and volume-of-fluid method". *Physics of Fluids, 17*(112103).

[4] Astrom, K. J., and Eklund, K., 1972. "A simplified non-linear model of a drum boiler-turbine unit". *International Journal of Control, 16*, pp. 145–169.

[5] Astrom, K. J., and Eklund, K., 1975. "A simple non-linear drum-boiler model". *International Journal of Control, 22*, pp. 739–740.

[6] Astrom, K. J., and Bell, R. D., 2000. "Drum-boiler Dynamics". *Automatica, 36*, pp. 363–378.

[7] Liu, J. Z., Yan, S., Zeng, D. L., Hu, Y., and Lv, Y., 2015. "A dynamic model used for controller design of a coal fired once-through boiler-turbine unit". *Energy, 93*, pp. 2069–2078.

[8] Changliang, L., Jizhen, L., Yuguang, N., and Weiping, L., 2001. "Nonlinear boiler model of 300MW power unit for system dynamic performance studies". *2001 IEEE International Symposium on Industrial Electronics Proceedings, ISIE 2001, Pusan, Korea*, pp. 1296–1300.

[9] Thompson, F. T., 1967. "A dynamic model of a drum-type boiler system". *IEEE Transactions on Power Apparatus and Systems, 86*(5), pp. 625–635.

[10] de Mello, F. P., 1991. "Boiler models for system dynamic performance studies". *IEEE transactions on Power Systems,* *6*(1), pp. 66–74.

[11] Kwan, H. W., and Anderson, J. H., 1970. "A mathematical model of a 200 MW boiler". *International Journal of Control,* *12*(6), pp. 977–998.

[12] Ibrahim, T. K., and Rahman, M. M., 2013. "Study on Effective Parameter of the Triple-Pressure Reheat Combined Cycle Performance". *Thermal Science,* *17*(2), pp. 497–508.

[13] Moran, M. J., Shapiro, H. N., Boettner, D. D., and Bailey, M. B., 2010. *Fundaments of Engineering Thermodynamics*, 7 ed. John Wiley & Sons, Inc., Hoboken, NJ.

[14] White, F. M., 2011. *Fluid Mechanics*, 7 ed. McGraw-Hill, New York, NY.